



**HAL**  
open science

## Disequilibrium $\delta^{18}\text{O}$ values in microbial carbonates as a tracer of metabolic production of dissolved inorganic carbon

Caroline Thaler, Christian Millo, Magali Ader, Carine Chaduteau, François Guyot, Bénédicte Ménez

► **To cite this version:**

Caroline Thaler, Christian Millo, Magali Ader, Carine Chaduteau, François Guyot, et al.. Disequilibrium  $\delta^{18}\text{O}$  values in microbial carbonates as a tracer of metabolic production of dissolved inorganic carbon. *Geochimica et Cosmochimica Acta*, 2017, 199, pp.112-129. 10.1016/j.gca.2016.10.051 . insu-03748877

**HAL Id: insu-03748877**

**<https://insu.hal.science/insu-03748877>**

Submitted on 26 Jan 2023

**HAL** is a multi-disciplinary open access archive for the deposit and dissemination of scientific research documents, whether they are published or not. The documents may come from teaching and research institutions in France or abroad, or from public or private research centers.

L'archive ouverte pluridisciplinaire **HAL**, est destinée au dépôt et à la diffusion de documents scientifiques de niveau recherche, publiés ou non, émanant des établissements d'enseignement et de recherche français ou étrangers, des laboratoires publics ou privés.

## Accepted Manuscript

Disequilibrium  $\delta^{18}\text{O}$  values in microbial carbonates as a tracer of metabolic production of dissolved inorganic carbon

Caroline Thaler, Christian Millo, Magali Ader, Carine Chaduteau, François Guyot, Bénédicte Ménéz

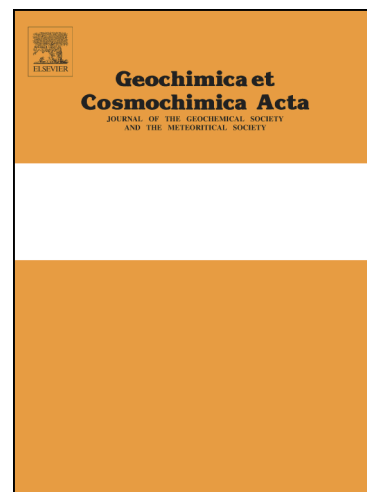
PII: S0016-7037(16)30654-8  
DOI: <http://dx.doi.org/10.1016/j.gca.2016.10.051>  
Reference: GCA 10020

To appear in: *Geochimica et Cosmochimica Acta*

Received Date: 3 September 2015  
Revised Date: 12 October 2016  
Accepted Date: 29 October 2016

Please cite this article as: Thaler, C., Millo, C., Ader, M., Chaduteau, C., Guyot, F., Ménéz, B., Disequilibrium  $\delta^{18}\text{O}$  values in microbial carbonates as a tracer of metabolic production of dissolved inorganic carbon, *Geochimica et Cosmochimica Acta* (2016), doi: <http://dx.doi.org/10.1016/j.gca.2016.10.051>

This is a PDF file of an unedited manuscript that has been accepted for publication. As a service to our customers we are providing this early version of the manuscript. The manuscript will undergo copyediting, typesetting, and review of the resulting proof before it is published in its final form. Please note that during the production process errors may be discovered which could affect the content, and all legal disclaimers that apply to the journal pertain.



**DISEQUILIBRIUM  $\delta^{18}\text{O}$  VALUES IN MICROBIAL CARBONATES AS A TRACER OF METABOLIC PRODUCTION OF DISSOLVED INORGANIC CARBON.**

**Caroline Thaler<sup>a,b</sup>, Christian Millo<sup>a,b,c</sup>, Magali Ader<sup>a,b</sup>, Carine Chaduteau<sup>a</sup>, François Guyot<sup>a,b,d</sup>, Bénédicte Ménéz<sup>a,b</sup>**

<sup>a</sup> Institut de Physique du Globe de Paris,

Sorbonne Paris Cité,

Univ Paris Diderot,

CNRS,

F-75005 Paris, France.

<sup>b</sup> Centre de Recherches sur le Stockage Géologique du CO<sub>2</sub>

(IPGP/TOTAL/SCHLUMBERGER/ADEME)

F-75005 Paris, France.

<sup>c</sup> now at Instituto Oceanográfico

Universidade de São Paulo

05508-900 São Paulo (SP), Brazil.

<sup>d</sup> now at Muséum National d'Histoire Naturelle

IMPMC UMR 7590 CNRS UPMC MNHN IRD Sorbonne Universités

57 Rue Cuvier, F-75005 Paris, France.

\* Corresponding author:

*E-mail address:* [caroline.thaler@mnhn.fr](mailto:caroline.thaler@mnhn.fr)

Thaler et al.,

Present address: UMR 7207 CNRS UPMC MNHN IRD Sorbonne Universités

CR2P, 57 Rue Cuvier, F-75005 Paris, France.

Keywords: Oxygen isotopes, biomineralization, carbonates, microbial carbonation, vital effect, isotopic Disequilibrium.

ACCEPTED MANUSCRIPT

**Abstract**

Carbon and oxygen stable isotope compositions of carbonates are widely used to retrieve paleoenvironmental information. However, bias may exist in such reconstructions as carbonate precipitation is often associated with biological activity. Several skeleton-forming eukaryotes have been shown to precipitate carbonates with significant offsets from isotopic equilibrium with water. Although poorly understood, the origin of these biologically-induced isotopic shifts in biogenic carbonates, commonly referred to as “vital effects”, could be related to metabolic effects that may not be restricted to mineralizing eukaryotes. The aim of our study was to determine whether microbially-mediated carbonate precipitation can also produce offsets from equilibrium for oxygen isotopes. We present here  $\delta^{18}\text{O}$  values of calcium carbonates formed by the activity of *Sporosarcina pasteurii*, a carbonatogenic bacterium whose ureolytic activity produces ammonia (thus increasing pH) and dissolved inorganic carbon (DIC) that precipitates as solid carbonates in the presence of  $\text{Ca}^{2+}$ . We show that the  $1000\ln\alpha_{\text{CaCO}_3\text{-H}_2\text{O}}$  values for these bacterially-precipitated carbonates are up to 24.7‰ smaller than those expected for precipitation at isotopic equilibrium. A similar experiment run in the presence of carbonic anhydrase (an enzyme able to accelerate oxygen isotope equilibration between DIC and water) resulted in  $\delta^{18}\text{O}$  values of microbial carbonates in line with values expected at isotopic equilibrium with water. These results demonstrate for the first time that bacteria can induce calcium carbonate precipitation in strong oxygen isotope disequilibrium with water, similarly to what is observed for eukaryotes. This disequilibrium effect can be unambiguously ascribed to oxygen isotope disequilibrium between DIC and water inherited from the oxygen isotope composition of the ureolytically produced  $\text{CO}_2$ , probably combined with a kinetic isotope effect during  $\text{CO}_2$  hydration/hydroxylation. The fact that both disequilibrium effects are triggered by the metabolic production of  $\text{CO}_2$ , which is common in many microbially-mediated carbonation processes, leads us to propose that metabolically-induced offsets from isotopic equilibrium in microbial carbonates may be more common than previously considered. Therefore,

precaution should be taken when using the oxygen isotope signature of microbial carbonates for diagenetic and paleoenvironmental reconstructions.

ACCEPTED MANUSCRIPT

## 1. INTRODUCTION

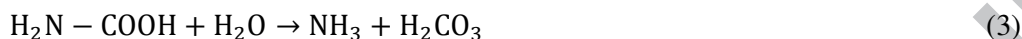
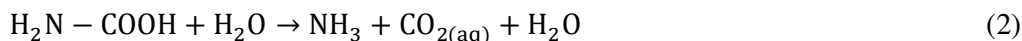
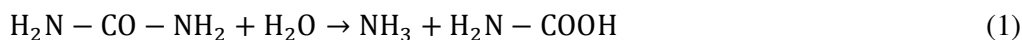
Oxygen isotopic composition in solid calcium carbonates ( $\delta^{18}\text{O}_{\text{CaCO}_3}$ ) precipitated at isotopic equilibrium with water (e.g., Epstein et al., 1953; O'Neil et al., 1969; Kim and O'Neil, 1997; Chacko and Deines, 2008) is a widely used proxy to estimate paleotemperature and isotopic composition of water (e.g., Urey, 1947; McCrea, 1950; Mook, 1971; Erez and Luz, 1983). Among these carbonates, microbially induced carbonates (Dupraz et al., 2008) have been used for paleoenvironmental or diagenetic reconstructions when assumed to precipitate at isotope equilibrium with the precipitating fluid (Pazdur et al., 1988; Chafetz and Lawrence, 1994; Andrews et al., 1997; Burns, 1998). Microbial activities can induce carbonate precipitation in several ways (i) pH and/or ionic concentrations (including dissolved inorganic carbon (DIC) species and divalent cations) in the surrounding medium can be increased by the microbial metabolic activity which favors carbonate precipitation (Castanier et al., 1999; Van Lith et al., 2003), (ii) organic matrices in the form of cell membranes or extracellular polymeric substances can serve as templates controlling carbonate nucleation and growth (Aloisi et al., 2006) and (iii) the DIC involved in carbonate precipitation can partly derive from microbial metabolic activity (Mortimer and Coleman, 1997). Microbially induced carbonates are common in nature (e.g. Riding, 2000) and can be found in some sedimentary carbonate concretions (Coleman and Raiswell, 1995; Sass et al., 1991; DeCraen et al., 1999), evaporitic carbonates (Guido et al., 2007), speleothems (Cacchio et al., 2004; Baskar et al., 2006; Rusznyak et al., 2012), soil carbonates (Cerling and Quade, 1993), dolomite deposits (Vasconcelos et al., 2005; Wacey et al., 2007), and within a fair proportion of Precambrian sedimentary rocks (e.g., Grotzinger, 1989).

However, it has become apparent that microbially induced carbonates may present disequilibrium  $\delta^{18}\text{O}$  values and it has been hypothesized that their  $\delta^{18}\text{O}$  values could reflect chiefly metabolic activity rather than environmental conditions (Mortimer and Coleman, 1997; De Craen et al., 1999; Gradzinski, 2003; Johnson et al., 2013). These isotopic shifts are similar to the “vital Thaler et al.,

effects” (Urey et al., 1951) identified in skeleton forming marine organisms. Several biological processes may result in vital effects but the underlying mechanisms remain controversial (e.g., McConnaughey, 1989a; Spero et al., 1997; Adkins et al., 2003; Weiner and Dove 2003; Ziveri et al., 2003; Thiagarajan et al., 2011). Among these mechanisms, the ones controlling carbonate precipitation rate (Epstein et al., 1953; Erez, 1978) and DIC speciation have often been invoked (e.g., McCrea, 1950; Zeebe, 1999; Adkins et al., 2003). It has also been hypothesized that the observed isotopic disequilibria could originate from an isotopic disequilibrium between DIC and water within the organism (McConnaughey, 1989a, b; McConnaughey et al., 1997; Furla et al., 2000), which could be induced by two major mechanisms: (i) the kinetic isotopic effect associated with hydration and/or hydroxylation of dissolved CO<sub>2</sub> (CO<sub>2(aq)</sub>), that occur at the site of carbonate precipitation and can produce a DIC with δ<sup>18</sup>O values in strong disequilibrium with water (Létolle et al 1990; McConnaughey, 2003; Rollion-Bard et al., 2003) and (ii) the metabolic production of DIC, which has been demonstrated to be responsible for most of C-isotope vital effects (Craig, 1953; Grossman, 1987; McConnaughey, 1989a, b; McConnaughey et al., 1997; Furla et al., 2000), but is considered as irrelevant for O-isotope vital effects, since DIC is assumed to readily reequilibrate isotopically with water. These hypotheses, invoked to explain oxygen vital effects could also explain isotopic shifts in microbially induced carbonates, as microbial activity modifies carbonate nucleation and precipitation rate, and affects DIC concentration, speciation and isotopic composition.

With the aim of further investigating this hypothesis, we performed biomineralization experiments using the ureolytic strain *Sporosarcina pasteurii*, a laboratory model microorganism of microbial carbonatogenesis (Ferris et al., 2003; Mitchell and Ferris, 2005; Dupraz et al., 2009a, b). *S. pasteurii* induces urea hydrolysis through the enzymatic activity of an urease enzyme and uses this reaction for energy generation (Mobley and Hausinger, 1989; Smith et al., 1993; Jahns, 1996) and in some cases for nitrogen assimilation (Nielsen et al., 1998; Swensen and Bakken, 1998). Ureolysis is performed in two steps (Andrews et al., 1984): (i) the production of ammonia and

carbamate from urea (Eq.(1)), which is catalyzed by urease and is rate limiting, and (ii) the rapid and spontaneous hydrolysis of carbamate into ammonia and  $\text{CO}_{2(\text{aq})}$  (Eq.(2)) (Krebs and Roughton, 1948; Matsuzaki et al., 2013) or  $\text{H}_2\text{CO}_3$  (Eq.(3)) (Mobley and Hausinger, 1989; Krajewska, 2009).



The produced ammonia equilibrates with water to yield ammonium (Eq.(4)), hence increasing pH. As pH increases,  $\text{CO}_{2(\text{aq})}$  (when formed through Eq.(2)) will either be hydrated to form carbonic acid (Eq.(5)) or hydroxylated to form bicarbonate ion (Eq.(6)), both of which being eventually converted into  $\text{CO}_3^{2-}$  at appropriate pH values.



The overall ureolysis reaction can hence be written as follows (Eq.(7)) (Ferris et al., 2003):



In the presence of calcium above a critical supersaturation level, calcium carbonate precipitation follows (Eq.(8)):



Three of these reactions can potentially induce oxygen isotope disequilibria between precipitated carbonates and water, namely:

(i) Ureolysis (Eqs.(1) and (2) or Eqs.(1) and (3)): The oxygen isotope composition of  $\text{CO}_{2(\text{aq})}$  or  $\text{H}_2\text{CO}_3$  produced by ureolysis is expected to depend on both the oxygen isotope composition of urea and the oxygen isotope fractionations of the successive reactions expressed in Eq.(1) and Eq.(2) (or Eq.(3)). The  $\delta^{18}\text{O}$  of the ureolytically produced  $\text{CO}_{2(\text{aq})}$  (or  $\text{H}_2\text{CO}_3$ ) will thus reflect its metabolic origin.

(ii)  $\text{CO}_{2(\text{aq})}$  hydration/hydroxylation (Eqs.(5) and (6)): Oxygen isotope composition of the produced DIC should vary as a function of the reactions involved (hydration or hydroxylation) (Létolle et al., 1990; McConnaughey, 2003; Rollion-Bard et al., 2003). At oxygen isotope equilibrium, the  $\delta^{18}\text{O}_{\text{OH}^-}$  value is a few tens of per mil lower than the  $\delta^{18}\text{O}_{\text{H}_2\text{O}}$  value (Green and Taube, 1963), so that the kinetic isotope fractionation associated with hydroxylation (favored at alkaline pH) is much higher than the one associated with hydration (Rollion-Bard et al., 2003).

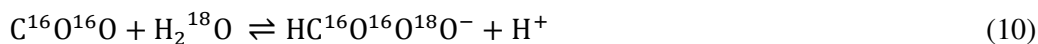
For both ureolysis and hydration/hydroxylation reactions, provided that the residence time of DIC in water before its precipitation as solid carbonates is too short to allow full O isotope equilibration (Beck et al., 2005), solid carbonates will inherit their oxygen isotopic signature from the disequilibrium  $\delta^{18}\text{O}_{\text{DIC}}$  value.

(iii) Carbonate precipitation (Eq.(8)): Kinetic fractionation can also occur during anion transfer from the solution to the growing crystal surface. Kinetic fractionation may be related to the precipitation rate (Dietzel et al., 2009; Gabitov et al., 2012; Watkins et al., 2013) or to a bacterially-influenced effect such as an organic template influence on nucleation and crystal growth, and the precipitation of an amorphous precursor phase.

In the following, we compare and discuss  $\delta^{18}\text{O}$  values obtained from two companion experiments of carbonate precipitation induced by bacterial ureolysis. The first experiment was performed by Millo et al. (2012), where only the carbon isotope systematics of bacterial ureolysis was dealt with. The  $1000\ln\alpha_{\text{CaCO}_3\text{-H}_2\text{O}}$  values between water and solid carbonates from the Millo et al. (2012) experiment are presented here for the first time. They are 24.7‰ smaller than the value expected at oxygen isotope equilibrium with water (Kim and O'Neil, 1997). The second experiment was conducted specifically for this study, with the aim of characterizing the mechanism responsible for the observed oxygen isotope disequilibrium. For this purpose, calcium carbonate precipitation induced by *S. pasteurii* was performed under experimental conditions identical to the ones described in Millo et al. (2012) but in the presence of the enzyme carbonic anhydrase (CA). CA has the ability to catalyze inter-conversion between  $\text{CO}_{2(\text{aq})}$  and  $\text{HCO}_3^-$  in aqueous solution (Eq.(9))

Thaler et al.,

(e.g., Lindskog and Coleman, 1973; Lindskog, 1997) thereby inducing oxygen isotope equilibrium between H<sub>2</sub>O and DIC (Eq.(10)) (e.g., Uchikawa and Zeebe, 2012):



A detailed comparison of the mineral byproducts, chemical features and oxygen isotope compositions obtained in both experiments is given and discussed in terms of the mechanisms responsible for oxygen isotope disequilibrium. The carbon isotope systematics of the experiment with CA, which reproduces fairly well the results of the experiment performed by Millo et al., (2012) without CA, is detailed in Appendixes B3 to B7.

## 2. EXPERIMENTAL SETTING AND SAMPLING PROTOCOL

### 2.1. Growth of bacteria and preparation of inoculum

*S. pasteurii* (strain ATCC 11859) was grown at 30°C in Brain Heart Broth (Merck) complemented with 0.3 M urea (Normapur, Prolabo). This inoculated growth medium was agitated for one day at 200 rounds per minute (rpm). An aliquot of this preculture was used for a second inoculation in the same medium, followed by agitation overnight under the same conditions, in order for bacteria to attain their stationary growth phase.

Bacterial cells were collected by centrifugation (8500 rpm for 10 minutes) and washed in sterile ultrapure water (UPW; resistivity = 18 MΩ·cm). Bacterial cells were then suspended in UPW at an optical density of 0.200 ± 0.005 at 600 nm (OD<sub>600</sub>). The bacterial suspension was subsequently used to inoculate the assays of the batch experiment, as described in section 2.4.

### 2.2. Artificial Ground Water

The precipitation experiments were performed in an artificial ground water (AGW) medium with a chemistry based on that of the groundwater of the Dogger aquifer (Paris Basin) (Azaroual et al., 1997). The rationale for this choice was to lay the basis for future field carbonation experiments in this French aquifer, a potential target site for CO<sub>2</sub> geological storage (Dupraz et al., 2009a, b). We simplified the protocol described in Millo et al. (2012) for the preparation of AGW: instead of using carbonate salts (KHCO<sub>3</sub> and NaHCO<sub>3</sub>) and then removing HCO<sub>3</sub><sup>-</sup> by HCl titration (and subsequent CO<sub>2</sub> outgassing), we used non-carbonated salts (NaCl and KCl) to obtain an AGW devoid of any initial DIC. This procedural change did not affect the final ionic composition of AGW, which was similar in both experiments. AGW was prepared at double strength in order to be mixed in equal parts with the bacterial suspensions at the beginning of the precipitation experiment. Double strength composition of AGW was the following: NaCl (80 mM), KCl (4 mM), MgSO<sub>4</sub>·7H<sub>2</sub>O (16 mM), CaCl<sub>2</sub> (40 mM), urea (Normapur, Prolabo) (66.7 mM). The same urea stock, with a δ<sup>13</sup>C<sub>0\_urea</sub> value of -48.9‰ (Millo et al., 2012), was used in both experiments. The solution was left to equilibrate freely with atmospheric CO<sub>2</sub>. Final pH was 6.0. The AGW ionic strength was 0.222 M, as calculated using the geochemical software JCHESS<sup>®</sup> (version 2.0; default CHESS<sup>®</sup> database version 2.5; Van der Lee, 1998), based on the AGW chemical composition and assuming a closed system with no gas–solution exchange at ambient temperature. After sterilization by filtration (with 0.2 µm Isopore<sup>™</sup>), AGW was stored at 4°C. Before the experiment, AGW was left to equilibrate thermally with ambient temperature. 2 mg/L of the CA enzyme was added to AGW before being mixed with the inoculum.

### 2.3. Carbonic anhydrase enzymatic activity

Commercial CA powder from bovine erythrocytes (C3934) was obtained from Sigma-Aldrich Company (St Louis, MO, USA). CA enzymatic activity (i.e. its efficiency at converting CO<sub>2(aq)</sub> into H<sub>2</sub>CO<sub>3</sub>, thus favoring CO<sub>2(g)</sub> dissolution) was quantified using the modified version of Thaler et al.,

the Wilbur-Anderson assay (Wilbur and Anderson, 1948). One hundred mL of 20 mM tris sulfate buffer were prepared and pH was adjusted to 8.3 by adding 110  $\mu\text{L}$  of  $(\text{NH}_2)_2\text{SO}_4$  at 25°C. The buffer was stored in ice. A  $\text{CO}_{2(\text{aq})}$ -saturated  $\text{H}_2\text{O}$  solution was prepared by bubbling  $\text{CO}_{2(\text{g})}$  through 200 mL of deionized water in ice for 30 minutes. Immediately prior to use, 1 mg/mL of CA was diluted to 0.01 mg/mL in cold deionized water.

An assay was run, consisting of successive pH measurements in 3 mL of buffer after addition of 2 mL of  $\text{CO}_{2(\text{aq})}$ -saturated  $\text{H}_2\text{O}$ , with or without simultaneous addition of 50  $\mu\text{L}$  CA solution. The enzymatic activity of CA (in Units/mg of protein or U/mg) was calculated based on the comparison between the time intervals required for pH to decrease from 8.3 to 6.3, with and without CA.

As Arashisar et al. (2004) demonstrated that ammonium and urea (both present in our experiments) can inhibit CA activity, we also performed the enzymatic activity assay in the presence of urea (at 2 g/L, i.e., the starting concentration in our experiments) or ammonium (at 1.2 g/L, the maximum value of dissolved inorganic nitrogen, DIN, produced in our precipitation experiment as a result of urea hydrolysis). We observed that the enzymatic activity of CA was equal to 2787 U/mg in the absence of urea and ammonium, 2331 U/mg in the presence of urea, and 2314 U/mg in the presence of ammonium.

#### **2.4. Batch experiment of bacterial ureolysis and associated $\text{CaCO}_3$ precipitation**

Bacterial ureolysis and associated  $\text{CaCO}_3$  precipitation in the experiment with CA were conducted in 12 mL Exetainer<sup>®</sup> vials (as in the experiment without CA of Millo et al., 2012). Exetainers<sup>®</sup> were filled with 6 mL AGW aliquots (containing CA) and inoculated under sterile conditions with 6 mL of bacterial suspension at  $t_0$ , so that no headspace remained. Vials were immediately capped with rubber septa, preventing any gaseous exchange with the atmosphere.

Inoculation resulted in a 1:1 mixing between AGW and bacterial suspension, decreasing  $OD_{600}$  from 0.200 to  $0.100 \pm 0.010$  and CA concentration from 2 to 1 mg/L in all experimental assays.

Inoculated assays (initially at ambient temperature) were placed onto a gyratory shaker (200 rpm) at a temperature of 30°C. Given that the first carbonate crystals appeared after ~ 30 minutes and that only 4% of the total carbonates precipitated after ~ 80 minutes, it is reasonable to assume that precipitation occurred at 30°C throughout the experiment.

Sacrificial sampling was carried out every 10 minutes during the first 30 minutes, then every 15 minutes during the following 2 hours, and finally every 30 minutes during the remaining 5h30. A control assay was also sacrificed in triplicate 24 hours after  $t_0$ .

At each sampling event, three 1 mL aliquots were syringed out through the vial cap rubber septum using sterile 0.22  $\mu\text{m}$  filters (Minisart<sup>®</sup>, Sartorius) in order to clear the samples from bacterial cells and minute  $\text{CaCO}_3$  crystals. These aliquots were used for  $\delta^{18}\text{O}$  measurement of water, for  $\delta^{13}\text{C}$  measurement of DIC, and for Ca concentration analysis, respectively. The remaining solution was carefully decanted and divided into two aliquots for pH and dissolved inorganic nitrogen concentration ( $\text{DIN} = \text{NH}_3 + \text{NH}_4^+$ ) measurements. Carbonate precipitates, formed at the bottom and on the wall of the vials, were immediately rinsed with a few drops of pure ethanol in order to dehydrate bacteria and prevent further ureolysis, further carbonate formation and/or dissolution–reprecipitation processes. After ethanol removal, vials were stored in an oven at 40°C to dry the precipitates overnight. The following day, vials were taken out of the oven, cooled to ambient temperature and weighed. The mass of precipitate was calculated either by weight difference relative to the empty vials or by calcium concentration measurements. The precipitation experiment in the presence of CA was repeated twice to confirm the results.

## 2.5. Chemical analysis and geochemical modelling

pH was measured using a HANNA HI 1131 (single junction) glass electrode calibrated following the three points procedure (HANNA Instruments PH210, precision =  $\pm 0.01$  pH unit) against certified pH buffer solutions (Fisher Chemical, precision =  $\pm 0.01$  pH unit) and without adjustments for the ionic strength. The electrode was rinsed with ultrapure water prior to and after each measurement, and stored in an acidic storage solution (KCl 3.5 M, pH  $\approx 4.0$ ) between each measurement to prevent solid carbonate deposition on the electrode itself.

The concentration of DIN was measured with a Shimadzu spectrophotometer (UV-1650 PC) with the Spectroquant<sup>®</sup> kit 1.14752.0001 ammonium test at 690 nm. The analytical uncertainty on DIN concentration was  $\pm 5\%$  ( $1\sigma$ ).

In the experiment without CA (Millo et al., 2012), the concentration of  $\text{Ca}^{2+}$  remaining in solution for each assay was derived from the concentration of Ca precipitated as  $\text{CaCO}_3$  and the initial  $\text{Ca}^{2+}$  concentration in solution ( $[\text{Ca}^{2+}]_0 = 20$  mM), while for the experiments with CA,  $\text{Ca}^{2+}$  concentration was measured by ion coupled plasma atomic emission spectroscopy (ICP-AES) using an Icap 6200 Series Thermo Fisher, yielding  $[\text{Ca}^{2+}]$  values with an analytical uncertainty of  $\pm 0.01$  mM ( $1\sigma$ ) ( $[\text{Ca}^{2+}]_0 = 20.6$  mM). The molar quantity of precipitated calcium carbonate ( $C_{\text{CaCO}_3}$ ) was inferred ( $\pm 0.05\%$  ( $1\sigma$ )) from  $[\text{Ca}^{2+}]$  values, which yielded the percentage of carbonate precipitation (%Precipitation) achieved in the course of the experiment.

The relative abundances of  $\text{CO}_3^{2-}$ ,  $\text{HCO}_3^-$  and  $\text{CO}_{2(\text{aq})}$  in solution were computed with the geochemical code JCHESS<sup>®</sup> (Van der Lee, 1998). AGW composition and experimental temperature ( $30^\circ\text{C}$ ) were chosen as input parameters assuming a closed system with no gas-solution exchange. Given that  $\text{Ca}^{2+}$  concentration decreases during the reaction, while those of total DIN and DIC increase, we adjusted the values of these input parameters at each computational step. We also adjusted the input concentrations of  $\text{OH}^-$  and  $\text{H}^+$  to model the measured pH variability and the concentration of Cl<sup>-</sup> in order to obtain electroneutrality.

## 2.6. DIC quantification and isotope analyses

Oxygen and carbon isotope compositions are reported in the usual  $\delta$  notation and expressed relative to the Vienna Standard Mean Ocean Water (V-SMOW) for oxygen and relative to the Vienna Pee Dee Belemnite (V-PDB) for carbon. Measured  $\delta$  values of  $\text{CaCO}_3$  and DIC were converted to the V-SMOW and V-PDB scales through calibration against three internal laboratory calcite standards. Their isotope composition was determined according to the method of McCrea (1950) using a Dual Inlet Finnigan<sup>TM</sup> Delta<sup>Plus</sup> XP isotope ratio mass spectrometer (Thermo Fisher Scientific) ( $\sigma = \pm 0.05\%$ ). Internal laboratory calcite standards were calibrated against the V-PDB reference using the international carbonate standards IAEA-CO-1 and NBS 19. Measured  $\delta^{18}\text{O}$  values of water were converted to the V-SMOW scale using three internal laboratory water standards calibrated against the V-SMOW and V-SLAP (Standard Light Arctic Precipitations) international reference materials. When necessary, conversion between the V-PDB and the V-SMOW scale was applied according to Coplen et al. (1983). Details of the procedure for  $\delta^{13}\text{C}$  and  $\delta^{18}\text{O}$  measurements are given in Appendixes B1 to B2. The analytical precision for  $\delta^{13}\text{C}$  and  $\delta^{18}\text{O}$  measurements was  $\pm 0.1\%$  ( $1\sigma$ ).

In the following sections, the isotope fractionation between two chemical species (A and B) will be expressed either as  $\alpha_{A-B}$ , the fractionation factor, or as  $1000\ln\alpha_{A-B}$ , where :

$$\alpha_{A-B} = \frac{10^3 + \delta_A}{10^3 + \delta_B} \quad (11)$$

[DIC] was quantified using the linear relationship between DIC concentration and intensity of the  $m/z$  44 peak provided by the mass spectrometer. The precision for [DIC] measurements was of  $\pm 5\%$  of the measured values ( $1\sigma$ ).

## 2.7. Scanning Electron Microscope imaging and mineralogical characterization of precipitates

Three samples of carbonate precipitates (sampled at 180, 300 minutes and 24 hours) selected

from the experiment with CA were examined under a Zeiss Ultra 55 FEG Scan Scanning Electron Microscope (SEM) equipped with a Gemini Column and an energy dispersive X-ray spectrometer (EDS) from Bruker operated at 15 kV and a working distance of 7.6 mm. Observations were made in secondary electrons (SE) and backscattered electrons (BSE) mode to document crystals morphology and obtain semi-quantitative information on crystal chemical composition.

We also performed X-Ray powder Diffraction (XRD) analysis on carbonate precipitates sampled at 240, 330, 450 minutes and 24 hours in the experiment with CA in order to characterize the carbonate mineralogy. The instrument (X'pert Pro MPD – diffractometer in theta-theta Bragg-Brentano geometry using Cu K $\alpha$  radiation) was operated with a step size of 0.017° 2 theta and a counting time of 400 s. Soller slits (0.04 rd) and anti-scatter slits were used.

### 3. RESULTS

#### 3.1. Evaluation of ureolysis kinetics

Urea consumption and hence ureolysis progress was quantified based on measured [DIN]. As shown in Table 1 and Fig. 1a, in the experiment with CA, [DIN] values increased at constant rate the first 200 minutes and then at a slower rate. The maximum measured [DIN] was 62.8 mM and was reached 24 hours after the beginning of the experiment whereas full urease consumption would have led to 66.6 mM of DIN. Therefore, over a time period of 24 hours, the ureolysis reaction did not proceed to completion in the experiment with CA as only 31.4 mM of urea were hydrolyzed at the end of the experiment while in the experiment without CA, all the urea (i.e., 33.3 mM) was hydrolyzed (Millo et al., 2012).

The kinetics of urea hydrolysis in the presence of ureolytic bacteria is often described by a first order rate law (Eq.(12)) (Ferris et al., 2003; Mitchell and Ferris, 2005; Fujita et al., 2008; Dupraz et al., 2009b):

Thaler et al.,

$$\frac{d[\text{urea}]}{dt} = -k_{\text{urea}}[\text{urea}] \quad (12)$$

where brackets denote concentration,  $t$  is time, and  $k_{\text{urea}}$  is the ureolysis rate constant. This law allowed  $k_{\text{urea}}$  calculation and hence the comparison of both experiment kinetics (with and without CA). According to Eq. (7),  $[\text{DIN}] = 2 [\text{urea}]$ . The rate constant  $k_{\text{urea}}$  (Eqs.(13) and (14)) was estimated from the temporal evolution of  $[\text{DIN}]$  and Eq. (12), according to:

$$[\text{DIN}] = 2[\text{urea}]_0(1 - e^{-k_{\text{urea}}t}) \quad (13)$$

$$k_{\text{urea}} = -\frac{\ln\left(1 - \frac{[\text{DIN}]}{2[\text{urea}]_0}\right)}{t} \quad (14)$$

where  $[\text{urea}]_0$  is the concentration of urea at  $t_0$ .

The derived  $k_{\text{urea}}$  value (Eq.(14)) determined with the least square method analysis was  $4.8 \pm 1.0 \text{ day}^{-1}$  ( $2\sigma$ ) in the experiment with CA. It was much lower than the one obtained for the experiment without CA for which a  $k_{\text{urea}}$  of  $8.2 \pm 1.2 \text{ day}^{-1}$  ( $2\sigma$ ) was calculated (Millo et al., 2012).

$[\text{DIN}]$  values exhibited some level of dispersion when plotted as a function of reaction time (Fig. 1a). For this reason, we followed the approach of Millo et al. (2012) and quantified the reaction yield by estimating the percentage of carbon from initial urea that was converted to inorganic carbon by ureolysis, a parameter hereafter referred to as Accumulated Carbon (referred to as Accumulated Product in Millo et al., 2012), the evolution of which, during the experiments with or without CA, is represented in Fig. 1b. The percentage of Accumulated Carbon (%AC) was calculated from the amount of carbon present in the DIC and in the  $\text{CaCO}_3$  precipitates, both deriving from urea carbon, following the equation:

$$\%AC = \frac{[\text{DIC}] + C_{\text{CaCO}_3}}{[\text{urea}]_0} \times 100 \quad (15)$$

Fig. 1b shows that %AC evolution as a function of time was less scattered than  $[\text{DIN}]$ , and %AC allowed us to monitor the progress of the ureolysis reaction with a better precision.

### 3.2. Chemistry

### 3.2.1. pH

The pH temporal evolution observed for the experiment with CA is reported in Table 1 and illustrated in Fig. 2a. At the beginning of the experiment (i.e., prior to microbial inoculation), pH of AGW was 6.0. After inoculation, pH rapidly increased to about 9.0 at a %AC value of 10%. Then, it decreased progressively to 8.4 (in correspondence to %AC = 60%) and finally increased again to around 8.7. The rapid pH increase at the onset of bacterial ureolysis is linked to the production of  $\text{NH}_4^+$  (Eq.(4)) and  $\text{HCO}_3^-$  (Eqs.(5) and (6)), as observed in previous studies (Ferris et al., 2003; Mitchell and Ferris, 2005; Dupraz et al., 2009b; Tobler et al., 2011). The subsequent pH decrease is due to  $\text{HCO}_3^-$  deprotonation and carbonate precipitation, the effect of which overwhelms the alkalinity increase induced by bacterial ureolysis. The slight pH increase at the end of the experiment (from %AC = 70% onwards) is induced by the continuation of the ureolysis reaction carried out by microbial cells having escaped carbonate encrustation and hence being still alive after precipitation (Dupraz et al., 2009a).

The pH variations observed in the presence of CA enzyme are similar to those observed in the absence of CA and reported in Millo et al. (2012), but on average 0.2 pH units lower. This is most likely due to the slower ureolysis kinetics observed in the presence of CA (section 3.1).

### 3.2.2. DIC and $\text{CaCO}_3$ precipitation

As expected and shown by black dots in Fig. 2b, [DIC] after inoculation increased in concert with %AC (at this stage only composed of DIC until the onset of  $\text{CaCO}_3$  precipitation). With the onset of  $\text{CaCO}_3$  precipitation, [DIC] reached a plateau between 5 and 7 mM when %AC = 30% and then increased again to reach 11.4 mM at the end of the experiment. Similar trends were observed in the experiment without CA (Millo et al., 2012), although in that experiment ureolysis proceeded to completion and thus produced more DIC (%AC = 100%; gray dots in Fig. 2b).

In the presence of CA, solid  $\text{CaCO}_3$  precipitation became quantifiable after 20 minutes of experiment, corresponding to a production of only 2% of AC, mostly as DIC (Table 1), whereas in the experiment without CA, solid  $\text{CaCO}_3$  precipitation became quantifiable after 100 minutes (Millo et al., 2012). In both experiments, the final  $C_{\text{CaCO}_3}$  value was comprised between 19.1 and 19.3 mM and was slightly lower than the initial calcium content of AGW. This indicates that only 90 to 95% of the AGW calcium content has precipitated as solid calcium carbonates during the experiments (Fig. 2c). As evidenced by the final  $[\text{Ca}^{2+}]$  values of 1.3 to 1.4 mM, some residual calcium remained in the medium. Calcium may also have been trapped as intracellular calcium phosphates within bacteria, as previously shown by Dupraz et al. (2009b).

### 3.3. Mineralogy of carbonate precipitates

SEM images showed that both morphology and size of solid carbonates changed in the course of the experiment. The samples collected after 180 minutes consisted mostly of smooth half spheres (5 to 10  $\mu\text{m}$  in diameter, more rarely 30  $\mu\text{m}$  in diameter) and of prisms (30 to 50  $\mu\text{m}$  edge length) (Fig. 3a). After 300 minutes of experiment, solid products were mostly made of aggregated crystals of intermediate shape ranging between spherical (70  $\mu\text{m}$  in diameter) and prismatic. *S. pasteurii* cell pockmarks resulting from cell lysis are present at the crystals surfaces (Fig. 3b). After 24 hours of experiment, carbonates consisted mainly of regular half spheres with smooth-cut faces (~70 to 100  $\mu\text{m}$  in diameter), presenting small cracks. Some crystals were bigger and presented a more irregular rhombohedral shape (Figs. 3c and d). These crystal morphologies were similar to those observed in the experiment without CA (Millo et al., 2012). XRD analyses of the carbonates precipitated at 240, 330, 450 minutes and 24 hours indicated an overwhelming dominance of calcite and low-Mg calcite ( $(\text{Mg}_{0.064}, \text{Ca}_{0.936})(\text{CO}_3)$ ), which represented 92 to 98% of the precipitates collected. Traces of vaterite (2 to 4%) were observed in all samples (except in the one collected 24 hours after the beginning of the experiment) and traces of aragonite (1 to 4%) were observed only in

precipitates collected 330 minutes to 24 hours after the beginning of the experiment (data not shown). This mineralogical composition was similar to that reported for the experiment without CA, where higher vaterite content was nonetheless observed during the initial stage of precipitation (Millo et al., 2012).

### 3.4. Calculations of precipitation rate $R$

The precipitation rates have been estimated in order to assess a possible effect of crystal growth rate on the  $\delta^{18}\text{O}$  values of solid carbonates (Dietzel et al., 2009; Watkins et al., 2013). The precipitation rate  $R$ , given in  $\mu\text{mol}/\text{m}^2\cdot\text{h}$ , is expressed conventionally as  $\log R$  according to the formulas given in Romanek et al. (1992), Jiménez-López et al. (2001), Tang et al. (2008), and Millo et al. (2012). Because our aim was to investigate the effect of precipitation rate on carbonate  $\delta^{18}\text{O}$  values throughout precipitation, we calculated an instantaneous  $\log R$  (Eq. (16)):

$$\log R = \frac{\Delta n_{\text{CaCO}_3}}{\Delta t \times \text{Sp}_{\text{CaCO}_3} \times m_{\text{CaCO}_3}} \quad (16)$$

where  $\Delta n_{\text{CaCO}_3}$  corresponds to the incremental quantity of  $\text{CaCO}_3$  (in  $\mu\text{mol}$ ) precipitated during  $\Delta t$  (in minutes),  $m_{\text{CaCO}_3}$  corresponds to the total mass of  $\text{CaCO}_3$  (in mg) accumulated at  $t$ , and  $\text{Sp}$  corresponds to the specific surface area of crystals, defined as follows (Eq. (17)).

$$\text{Sp}_{\text{CaCO}_3} = \frac{S_{\text{mineral}}}{V_{\text{mineral}} \times \rho_{\text{mineral}}} \quad (17)$$

$S_{\text{mineral}}$ ,  $V_{\text{mineral}}$  and  $\rho_{\text{mineral}}$  are respectively the surface, volume and density of representative minerals of averaged size at time  $t$ . Surface and volume were derived from SEM observations, which allowed us to estimate the size and shape of the precipitated grains that were assimilated to spheres or cubes (see section 3.3). The dominant Ca-carbonate polymorph was identified by XRD analysis at each stage. From these observations, along with previously established systematics (Millo et al., 2012), we considered that the initial solid phase dominating during the first 50 minutes consisted in 5  $\mu\text{m}$  diameter spherical aggregates of vaterite crystals. They were still visible on the

SEM images of carbonates collected at  $t = 180$  minutes (Fig. 3a) but not in the SEM images of carbonates collected later. After 50 minutes of experiment, solid carbonates occurred mostly in the form of aggregates of calcite crystals, whose shapes were approximated to cubes. Such a successive vaterite and calcite precipitation stages were consistent with the evolution of the saturation index obtained for the different carbonate phases (Appendix A1). Saturation index showed in particular that after 50 minutes of experiment calcite became the most thermodynamically favourable calcium carbonate polymorph, followed by aragonite and vaterite.

Considering that Figure 3a (displaying solid carbonates collected 180 min after the onset of precipitation) showed prisms of 30 to 50  $\mu\text{m}$  edge length and that Figures 3b, c and d (displaying solid carbonates collected from 300 min to 24 h of experiment) showed bigger prisms of 70 to 100  $\mu\text{m}$  edge length, two different averaged calcite prism edge lengths were considered as representative of the experiment: 30  $\mu\text{m}$  from 50 to 115 min, and 70  $\mu\text{m}$  from 115 min up to the end of the experiment. Edge length estimates for the experiment without CA are given in Millo et al. (2012).

Figure 4 shows precipitation rates obtained for the experiment with CA (black symbols) and compared to those observed in the absence of CA (grey symbols). In the experiment with CA,  $\log R$  increased from 4.8 to 5.6  $\mu\text{mol}/\text{m}^2\cdot\text{h}$ , then decreased to 4.4  $\mu\text{mol}/\text{m}^2\cdot\text{h}$ . In the experiment without CA,  $\log R$  increased from 3.9 at the beginning of precipitation to 5.0  $\mu\text{mol}/\text{m}^2\cdot\text{h}$ , before decreasing to 4.6  $\mu\text{mol}/\text{m}^2\cdot\text{h}$ . Except for the precipitation onset,  $\log R$  values were thus similar for both experiments.

### 3.5. $\delta^{18}\text{O}$ values of $\text{CaCO}_3$

The  $\delta^{18}\text{O}_{\text{CaCO}_3}$  values obtained in the presence and in the absence of CA are reported in Table 2 and the associated  $1000\ln\alpha_{\text{CaCO}_3\text{-H}_2\text{O}}$  values of are displayed in Fig. 5 as a function of the number of moles of accumulated  $\text{CaCO}_3$  ( $C_{\text{CaCO}_3}$ ) in order to facilitate data interpretation (see Thaler et al.,

calculations in section 4.2). In the presence of CA,  $\delta^{18}\text{O}_{\text{CaCO}_3}$  values were equal to 4.3‰ at the beginning of precipitation and increased progressively, reaching a plateau around 19‰ when 70% of  $\text{CaCO}_3$  have precipitated. In the experiment performed without CA, initial  $\delta^{18}\text{O}_{\text{CaCO}_3}$  values were equal to -5.4‰ and increased linearly with the amount of carbonate precipitated, reaching a  $\delta^{18}\text{O}_{\text{CaCO}_3}$  value of 0.1‰ at the end of precipitation.  $\delta^{18}\text{O}_{\text{CaCO}_3}$  values thus showed a marked difference between the experiments conducted with and without CA.

The  $\delta^{18}\text{O}_{\text{H}_2\text{O}}$  values were  $-6.8 \pm 0.1\text{‰}$  in the experiment with CA and  $-7.4 \pm 0.1\text{‰}$  in the experiment without CA and remained constant during the course of the experiments.

## 4. DISCUSSION

### 4.1. Ureolysis kinetics

Ureolysis exhibited slower reaction kinetics in the experiment with CA than in the experiment without CA (Fig. 1a). Since preliminary tests did not show any impact of the presence of CA on ureolysis kinetics (data not shown), the slower ureolysis kinetics observed in the experiment with CA reflects the fact that bacterial inoculum can be in a slightly different physiological state from one experiment to the other, as the AGW used for the experiments is not a growth medium but a minimum medium devoid of micronutrients and organic carbon (except for urea). As a consequence, bacteria inoculated in AGW can survive only during a limited time, during which they catalyse ureolysis. In the experiment with CA, the bacterial inoculum was in a slightly weaker physiological state as compared to the bacteria activity in the experiment without CA. Bacteria in a weaker physiological state at the time of inoculation have a weaker ureolytic activity, resulting in a slower ureolysis kinetics, a slower evolution of pH and a delayed onset of carbonate precipitation.

## 4.2. Comparing experimental $\delta^{18}\text{O}_{\text{CaCO}_3}$ values to the values predicted at isotopic equilibrium

The experimental and theoretical determinations of the oxygen isotope equilibrium fractionation between calcium carbonate and water ( $1000\ln\alpha_{\text{CaCO}_3\text{-H}_2\text{O}}$ ) converge toward values comprised within a 2‰ range at 30°C (Kim and O'Neil, 1997; Coplen, 2007; Chacko and Deines, 2008). We compared the  $1000\ln\alpha_{\text{CaCO}_3\text{-H}_2\text{O}}$  values between calcite and water obtained in our experiments with the equilibrium oxygen isotope fractionation factor (at 30°C) of Kim and O'Neil (1997), the one from the field study of Coplen (2007), and the one from the theoretical study of Chacko and Deines (2008) (Appendix C1). The three fractionation factors were expressed in terms of  $1000\ln\alpha_{\text{CaCO}_3\text{-H}_2\text{O}}$  and reported in Fig. 5 for visual comparison. The lowest  $1000\ln\alpha_{\text{CaCO}_3\text{-H}_2\text{O}}$  value is the one after Chacko and Deines (2008) (26.7‰), whereas the highest  $1000\ln\alpha_{\text{CaCO}_3\text{-H}_2\text{O}}$  value is the one after Coplen (2007) (28.8‰). Among those three studies, we mostly compare our results to Kim and O'Neil (1997) equilibrium fractionation factor, as it has been determined with an experimental approach that is the most comparable to our precipitation setup.

In the experiment without CA, initial  $1000\ln\alpha_{\text{CaCO}_3\text{-H}_2\text{O}}$  values were 24.7‰ smaller than expected for calcite at equilibrium with water (Kim and O'Neil, 1997) and remained at least 18‰ smaller than the value expected at equilibrium throughout the experiment. In the experiment with CA,  $1000\ln\alpha_{\text{CaCO}_3\text{-H}_2\text{O}}$  values were initially 16.0‰ smaller than predicted for calcite at equilibrium with water (Kim and O'Neil (1997) but increased progressively, approaching the equilibrium fractionation value predicted by Chacko and Deines (2008) at the end of the experiment (Fig. 5).

Based on  $\delta^{13}\text{C}$  data, Millo et al. (2012) demonstrated that after precipitation, solid carbonates did not reequilibrate their carbon isotopic composition with the continuously isotopically-evolving DIC (demonstration reproduced for the experiment with CA in Appendix B7). Given that carbon and oxygen isotope reequilibrations in solid carbonate occur through dissolution/reprecipitation processes (e.g., Mavromatis et al., 2015), it follows that in the present

experiments, solid carbonates did not undergo dissolution/precipitation. This, together with the fact that oxygen isotope equilibration within the carbonate system is slower than carbon isotope equilibration (Zeebe and Wolf-Gladrow, 2001) implies that, as for  $\delta^{13}\text{C}_{\text{CaCO}_3}$  values,  $\delta^{18}\text{O}_{\text{CaCO}_3}$  values reflect the mass and isotopic balance of the progressive accumulation of instantaneously precipitated  $\text{CaCO}_3$  ( $\delta^{18}\text{O}_{\text{inst.CaCO}_3}$ ) without any isotopic reequilibration. On this basis, we calculated  $\delta^{18}\text{O}_{\text{inst.CaCO}_3}$  values in order to verify that (i) carbonate precipitation occurred out of oxygen isotope equilibrium with water throughout the experiment without CA and (ii) carbonate precipitation occurred at oxygen isotope equilibrium with water at the end of the experiment with CA.

As no isotopic reequilibration occurred after precipitation, the  $\delta^{18}\text{O}$  value of accumulated  $\text{CaCO}_3$  ( $\delta^{18}\text{O}_{\text{acc.CaCO}_3}$ ) can be expressed as:

$$\delta^{18}\text{O}_{\text{acc.CaCO}_3} = \frac{1}{C_{\text{CaCO}_3} - C_0} \int_{C_0}^{C_{\text{CaCO}_3}} \delta^{18}\text{O}_{\text{inst.CaCO}_3} dC_{\text{CaCO}_3} \quad (18)$$

with  $C_0$  being the initial molar quantity of precipitated  $\text{CaCO}_3$  at the beginning of the experiment (in mM) and being equal to 0.

This allows the calculation of  $\delta^{18}\text{O}_{\text{inst.CaCO}_3}$  values, as follows:

$$\delta^{18}\text{O}_{\text{inst.CaCO}_3} = \frac{d[(C_{\text{CaCO}_3} - C_0)\delta^{18}\text{O}_{\text{acc.CaCO}_3}]}{dC_{\text{CaCO}_3}} \quad (19)$$

In order to calculate  $\delta^{18}\text{O}_{\text{inst.CaCO}_3}$  values, the evolution of  $\delta^{18}\text{O}_{\text{acc.CaCO}_3}$  values was first modeled by using a best-fit curve of the measured  $\delta^{18}\text{O}_{\text{CaCO}_3}$  values, in a  $\delta^{18}\text{O}_{\text{CaCO}_3}$  versus  $C_{\text{CaCO}_3}$  diagram for both experiments (Fig. 5). For the experiment with CA, the relationship between  $\delta^{18}\text{O}_{\text{acc.CaCO}_3}$  and  $C_{\text{CaCO}_3}$  was approximated by the following best-fit equation:

$$\delta^{18}\text{O}_{\text{acc.CaCO}_3} = \frac{a}{b(C_{\text{CaCO}_3})^d} + e \quad (20)$$

with  $a = -1.5$ ,  $b = 0.08$ ,  $d = 0.17$  and  $e = 30.4$ . Uncertainty for  $\delta^{18}\text{O}_{\text{acc.CaCO}_3}$  values was calculated to be of  $\pm 1.3\%$  with the least square method.

Combination of Eq. (20) with Eq. (19) yields:

$$\delta^{18}\text{O}_{\text{inst.CaCO}_3} = \frac{-15.56}{(\text{C}_{\text{CaCO}_3})^{0.17}} + 30.4 \quad (21)$$

Supposing that the main source of uncertainty in the calculation of  $\delta^{18}\text{O}_{\text{inst.CaCO}_3}$  values comes from the calculation of  $\delta^{18}\text{O}_{\text{acc.CaCO}_3}$  values, we estimated the uncertainty of  $\delta^{18}\text{O}_{\text{inst.CaCO}_3}$  values to be of the order of  $\pm 1.3\%$ .

For the experiment without CA, the best-fit function for  $\delta^{18}\text{O}_{\text{acc.CaCO}_3}$  values was:

$$\delta^{18}\text{O}_{\text{acc.CaCO}_3} = a'(\text{C}_{\text{CaCO}_3})^2 + b'(\text{C}_{\text{CaCO}_3}) + d' \quad (22)$$

With  $a' = 0.0054$ ,  $b' = 0.22$  and  $c' = -5.5$ . Uncertainty calculated from a least square regression for  $\delta^{18}\text{O}_{\text{acc.CaCO}_3}$  values was  $\pm 0.6\%$ .

Eq. (19) and Eq. (22) allow calculating  $\delta^{18}\text{O}_{\text{inst.CaCO}_3}$  values, according to:

$$\delta^{18}\text{O}_{\text{inst.CaCO}_3} = 0.0162(\text{C}_{\text{CaCO}_3})^2 + 0.44(\text{C}_{\text{CaCO}_3}) - 5.5 \quad (23)$$

with an uncertainty of  $\pm 0.6\%$  evaluated from least square regression.

We then established the evolution of the  $1000\ln\alpha_{\text{CaCO}_3\text{inst-H}_2\text{O}}$  curves (with or without CA) shown in Fig. 5 whose errors were  $\pm 1.4\%$  for the calculation with CA and  $\pm 0.7\%$  for the calculation without CA.

In the experiment without CA, calculated  $1000\ln\alpha_{\text{CaCO}_3\text{inst-H}_2\text{O}}$  values increased from  $1.9\%$  to  $16.3\% \pm 1.4\%$  ( $1\sigma$ ), while published equilibrium fractionation factors range from  $26.7\%$  to  $28.8\%$  at  $30^\circ\text{C}$  (Kim and O'Neil, 1997; Coplen, 2007; Chacko and Deines, 2008), indicating that  $\text{CaCO}_3$  always precipitated out of oxygen isotope equilibrium in the absence of CA. In contrast,  $1000\ln\alpha_{\text{CaCO}_3\text{inst-H}_2\text{O}}$  values calculated for the experiment in the presence of CA reached a final  $1000\ln\alpha_{\text{CaCO}_3\text{inst-H}_2\text{O}}$  value of  $27.6\% \pm 1.4\%$  ( $1\sigma$ ), that lies between Kim and O'Neil (1997) and Coplen, (2007) equilibrium fractionation factors (Fig. 5).

Overall, comparison of both experiments unambiguously showed that in the experiment without CA, a very strong oxygen isotope disequilibrium between precipitated carbonate and water

can be observed. This disequilibrium was suppressed in the experiment with CA as a result of the enzyme activity. Note however that, given the fact that our equilibrium value was calculated assuming that mineral precipitates were composed of 100% calcite, whereas traces of aragonite and vaterite have been evidenced using SEM and XRD, and given the relatively poor precision of our equilibrium  $1000\ln\alpha_{\text{CaCO}_3\text{-H}_2\text{O}}$  value, our study cannot bring accurate constraints on the oxygen isotope equilibrium fractionation factor values for calcite precipitation.

#### 4.3. Disequilibrium $\delta^{18}\text{O}$ recorded in calcium carbonates in the absence of CA

Ureolysis-induced  $\text{CaCO}_3$  precipitation in the absence of CA resulted in initial  $1000\ln\alpha_{\text{CaCO}_3\text{-H}_2\text{O}}$  values 24.7‰ smaller than the ones expected for oxygen isotope equilibrium with water (Kim and O'Neil, 1997) (Fig. 5). To the best of our knowledge, such a strong offset from equilibrium has never been reported for microbial carbonates. Several potential reasons could explain deviations from oxygen isotope equilibrium:

- (1) Kinetic fractionation of oxygen isotopes induced by a high  $\text{CaCO}_3$  precipitation rate, hence promoting the incorporation of  $^{18}\text{O}$ -depleted  $\text{CO}_3^{2-}$  in the precipitated  $\text{CaCO}_3$  (Eq.(8));
- (2) Changes in calcium carbonate mineralogy (polymorphisms) during precipitation;
- (3) pH effect;
- (4) Kinetic fractionation of oxygen isotopes during  $\text{CO}_{2(\text{aq})}$  hydration or hydroxylation (Eqs.(5) and (6) if  $\text{CO}_2$  is produced by ureolysis), thereby promoting the formation of  $^{18}\text{O}$ -depleted  $\text{H}_2\text{CO}_3$  or  $\text{HCO}_3^-$ ;
- (5) Kinetic fractionation of oxygen isotopes associated with the two successive steps of the ureolysis reaction (Eq.(1) and Eq.(2) or (3)) superimposed to the oxygen isotope ratio of urea, which could promote the formation of  $^{18}\text{O}$ -depleted  $\text{H}_2\text{CO}_3$  or  $\text{CO}_{2(\text{aq})}$  (Eqs. (1), (2) and (3));

If disequilibrium had resulted from a preferential entrapment of isotopically light oxygen in the solid carbonate due to fast crystal growth (hypothesis (1)), we should have observed offsets from the isotopic equilibrium range in the experiment conducted in the presence of CA, as this enzyme has no influence on the precipitation process. In that case, we calculated that, for both experiments, precipitation rate would have led to a  $1000\ln\alpha_{\text{CaCO}_3\text{-H}_2\text{O}}$  value 1.5‰ smaller than the equilibrium fractionation factor according to Dietzel et al. (2009) and 0.8‰ bigger than equilibrium fractionation factor according to Gabitov et al. (2012) (Appendix C1). Kinetic fractionation of oxygen isotopes resulting from high  $\text{CaCO}_3$  precipitation rate can therefore be ruled out as a possible explanation for the 16.0‰ and 24.7‰ differences observed between our experimental  $1000\ln\alpha_{\text{CaCO}_3\text{-H}_2\text{O}}$  values and equilibrium fractionation factors (according to Kim and O'Neil, 1997) even though our precipitation rates are particularly high for a biologically-induced precipitation.

Because the presence of CA does not induce neither mineralogical changes nor recrystallization processes, hypothesis (2) also appears unsuitable to explain the difference in  $\delta^{18}\text{O}_{\text{CaCO}_3}$  values observed in the two experiments. Moreover, calcite, vaterite and aragonite precipitated at oxygen isotope equilibrium have relatively similar  $\delta^{18}\text{O}$  values. At 30°C, both aragonite and vaterite are enriched in  $^{18}\text{O}$  relative to calcite; aragonite by 0.6‰ to 0.8‰ and vaterite by 0.5‰ to 0.6‰ (Tarutani et al., 1969; Kim and O'Neil, 1997). While these differences may have been preserved in the oxygen isotope composition of the carbonate precipitates, they are far too small to account for the 16.0‰ and 24.7‰ differences observed between equilibrium  $1000\ln\alpha_{\text{CaCO}_3\text{-H}_2\text{O}}$  values (according to Kim and O'Neil, 1997) and the  $1000\ln\alpha_{\text{CaCO}_3\text{-H}_2\text{O}}$  value obtained for the first precipitated carbonates in the experiments with and without CA, respectively.

The magnitude of pH effect (hypothesis (3)) can be calculated following the approach proposed by Zeebe (2007) assuming that DIC species are incorporated into the solid carbonate according to their proportions in the aqueous phase (Zeebe, 2007; Kim et al., 2014). In order to do

these calculations it is necessary to know the isotopic composition of each DIC species, which is possible by assuming that DIC is in oxygen isotope equilibrium with water. The results of the calculations (detailed in Appendix C2) performed for all the pH values measured during the experiment with CA (Table 1) correspond to  $1000\ln\alpha_{\text{CaCO}_3\text{inst}-\text{H}_2\text{O}}$  values ranging from 27.9 to 29.3‰, which is close to the 27.1‰ value estimated following Kim and O’Neil (1997). The pH effect would thus also be far too small to account for the -16.0‰ and -24.7‰ oxygen isotope disequilibrium observed between precipitated carbonate and water in the experiment with *S. pasteurii*.

Our results thus definitively point to an oxygen isotopic disequilibrium between the DIC produced by ureolysis and water (hypotheses (4) and (5)). The disequilibrium was recorded in our solid carbonates because the DIC residence time in solution was short enough to prevent its full oxygen isotope equilibration with water before its precipitation as  $\text{CaCO}_3$ . As an illustration, at pH 9, in the absence of CA, the isotope equilibration between DIC and water requires ~ 44h (Zeebe and Wolf-Gladrow, 2001) whereas most of our carbonates precipitated in less than 4 hours after the onset of the experiments. Moreover, DIC was produced progressively over the course of these 4 hours, hence further reducing the time available for isotopic equilibration. This disequilibrium between DIC and water is thus necessarily related directly or indirectly to ureolysis, the only source of DIC in the experiments. The disequilibrium may be inherited from the ureolysis reaction itself (hypothesis (5)) and/or from hydroxylation and hydration reactions if  $\text{CO}_{2(\text{aq})}$ , rather than  $\text{H}_2\text{CO}_3$ , is produced by ureolysis (Eqs. (1) and (2)) (hypothesis (4)).

If the ureolysis product is  $\text{CO}_{2(\text{aq})}$ , the contribution of hydration and hydroxylation to disequilibrium  $\delta^{18}\text{O}_{\text{HCO}_3^-}$  values can be estimated by isotopic mass balance calculations (Létolle et al., 1990; Usdowski et al., 1991; Clark et al., 1992):

$$\text{Hydroxylation: } \delta^{18}\text{O}_{\text{HCO}_3^-} = \frac{2}{3}\delta^{18}\text{O}_{\text{CO}_{2(\text{aq})}} + \frac{1}{3}\delta^{18}\text{O}_{\text{OH}^-} \quad (24)$$

$$\text{Hydration: } \delta^{18}\text{O}_{\text{HCO}_3^-} = \frac{2}{3}\delta^{18}\text{O}_{\text{CO}_{2(\text{aq})}} + \frac{1}{3}\delta^{18}\text{O}_{\text{H}_2\text{O}} \quad (25)$$

As the  $\delta^{18}\text{O}_{\text{CO}_2(\text{aq})}$  value could not be measured during our experiment, the  $\delta^{18}\text{O}_{\text{HCO}_3^-}$  value cannot be directly calculated. But we can at least evaluate if hydration and hydroxylation alone can account for the observed disequilibrium, assuming that  $\text{CO}_2(\text{aq})$  produced by ureolysis is in oxygen isotope equilibrium with water. To determine  $\delta^{18}\text{O}_{\text{CO}_2(\text{aq})}$  at equilibrium with water we used the equilibrium  $1000\ln\alpha_{\text{CO}_2(\text{aq})-\text{H}_2\text{O}}$  value (39.5‰ at 30°C) from Beck et al. (2005) and to determine the  $\delta^{18}\text{O}_{\text{OH}^-}$  value, we used the equilibrium  $1000\ln\alpha_{\text{H}_2\text{O}-\text{OH}^-}$  value (36.8‰ at 30°C) from Green and Taube, (1963). With a  $\delta^{18}\text{O}_{\text{H}_2\text{O}}$  value of -7.4‰ as in the experiment without CA (Table 2), we obtained  $\delta^{18}\text{O}_{\text{OH}^-} = -44.2\%$  and  $\delta^{18}\text{O}_{\text{CO}_2(\text{aq})} = -32.1\%$ .

At pH 9, which corresponds to the pH of the main carbonate precipitation phase in our experiments, approximately 76% of  $\text{CO}_2$  undergoes hydroxylation and 24% hydration (see Appendix C2 for calculations after Zeebe and Wolf-Gladrow (2001)).  $\delta^{18}\text{O}_{\text{HCO}_3^-}$  can then be calculated by weighing Eqs. (24) and (25):

$$\delta^{18}\text{O}_{\text{HCO}_3^-} = 0.76 \left[ \frac{2}{3} \delta^{18}\text{O}_{\text{CO}_2(\text{aq})} + \frac{1}{3} \delta^{18}\text{O}_{\text{OH}^-} \right] + 0.24 \left[ \frac{2}{3} \delta^{18}\text{O}_{\text{CO}_2(\text{aq})} + \frac{1}{3} \delta^{18}\text{O}_{\text{H}_2\text{O}} \right] \quad (26)$$

$$\delta^{18}\text{O}_{\text{HCO}_3^-} = 0.76 \left[ \frac{2}{3} (32.1) + \frac{1}{3} (-44.2) \right] + 0.24 \left[ \frac{2}{3} (32.1) + \frac{1}{3} (-7.4) \right]$$

This leads to a final  $\delta^{18}\text{O}_{\text{HCO}_3^-}$  value of 9.6‰ and thus to a disequilibrium  $1000\ln\alpha_{\text{HCO}_3^--\text{H}_2\text{O}}$  value of 17.0‰ while the equilibrium  $1000\ln\alpha_{\text{HCO}_3^--\text{H}_2\text{O}}$  is 30.1‰ at 30°C (Beck et al., 2005). With equilibrium initial conditions,  $\text{CO}_2(\text{aq})$  hydration and hydroxylation can explain a 13‰ offset from equilibrium for the  $1000\ln\alpha_{\text{HCO}_3^--\text{H}_2\text{O}}$  value whereas the initial offset from equilibrium observed in solid carbonates was -24.7‰ in the experiment with CA. This demonstrates that  $\text{CO}_2$  cannot be in oxygen isotope equilibrium with water when it is generated by ureolysis. Part or all of the disequilibrium must hence be associated with oxygen isotopic fractionation during ureolysis (hypothesis 5) resulting in the production of  $\text{CO}_2(\text{aq})$  (or  $\text{H}_2\text{CO}_3$ ) with  $\delta^{18}\text{O}$  lower than their equilibrium values with water.

If the ureolysis product is  $\text{H}_2\text{CO}_3$  (Eq. (1) and (3)), then the first precipitated carbonates before any DIC reequilibration with water have oxygen atoms directly inherited from the hydrolysis of urea, without any fractionation caused by hydration and hydroxylation. Because it was not possible to perform direct  $\delta^{18}\text{O}$  measurements of  $\text{H}_2\text{CO}_3$  or  $\text{CO}_{2(\text{aq})}$  produced by ureolysis, we can only provide qualitative constraints for them. Four parameters must be considered to constrain  $\delta^{18}\text{O}$  of  $\text{H}_2\text{CO}_3$  or  $\text{CO}_2$ : (i) the isotope composition of the parent urea which provide 1 out of the 2 or 3 oxygen atoms in the  $\text{CO}_2$  or  $\text{H}_2\text{CO}_3$  molecules, (ii) the oxygen isotope fractionation imparted to this oxygen by ureolysis, (iii) the oxygen isotope composition of water from which 1 or 2 out, of the 3 to 4 oxygen atoms in  $\text{CO}_{2(\text{aq})}$  or  $\text{H}_2\text{CO}_3$  molecules, come from and (iv) the oxygen isotope fractionation imparted to these O atoms by the hydration steps of ureolysis (Eq. 1,2 and 3).

The oxygen isotope composition of urea ( $\delta^{18}\text{O}_{\text{urea}}$ ) is not measurable with our experimental setup. However, because the procedure used for urea synthesis from ammonia and  $\text{CO}_2$  (Kishimoto et al., 2008) generates strongly negative  $\delta^{13}\text{C}$  values (a  $\delta^{13}\text{C}_{\text{urea}}$  of  $-48.9\%$  was measured for the urea used in our experiments) it is likely that the  $\delta^{18}\text{O}_{\text{urea}}$  value is negative as well. Similarly, since ureolysis generates  $^{12}\text{C}$ -enriched  $\text{H}_2\text{CO}_3$  with an enzymatic kinetic fractionation factor of  $-12.5\%$  for carbon isotopes (Millo et al., 2012; see Appendix B6 for further information), ureolysis-derived  $\text{H}_2\text{CO}_3$  (or  $\text{CO}_{2(\text{aq})}$ ) is likely to be  $^{16}\text{O}$ -enriched. Finally, the two successive hydrations steps of urea molecules should also incorporate in the product of ureolysis light oxygen isotopes coming from the water molecules. Overall, a kinetic fractionation associated with ureolysis could easily account for the whole isotopic disequilibrium between water and  $\text{CaCO}_3$  (and by extension DIC) observed for oxygen isotopes.

In the course of the experiment without CA,  $\delta^{18}\text{O}_{\text{CaCO}_3}$  values increased progressively, hence reducing the observed offset from oxygen isotope equilibrium values in the final stage of the experiment (Fig. 5). The  $\delta^{18}\text{O}_{\text{CaCO}_3}$  increase matched a comparable  $\delta^{13}\text{C}_{\text{CaCO}_3}$  increase, resulting in a significant  $\delta^{18}\text{O}_{\text{CaCO}_3}$  versus  $\delta^{13}\text{C}_{\text{CaCO}_3}$  correlation (Fig. 6) ( $R^2=0.872$  with a slope approximately

equal to 1). In our experiments, the only process suitable to account for the observed  $\delta^{18}\text{O}_{\text{CaCO}_3}$  versus  $\delta^{13}\text{C}_{\text{CaCO}_3}$  correlation in solid carbonates is Rayleigh distillation of urea during DIC-producing ureolysis, which would lead to a progressive  $^{18}\text{O}$  enrichment of the residual urea as observed for carbon isotopes (Millo et al., 2012). The  $\delta^{18}\text{O}_{\text{CaCO}_3}$  increase during ureolysis may thus result from the production of progressively  $^{18}\text{O}$ -enriched  $\text{H}_2\text{CO}_3$ . However, the correlation between the  $\delta^{18}\text{O}_{\text{CaCO}_3}$  and  $\delta^{13}\text{C}_{\text{CaCO}_3}$  values may also result from two distinct mechanisms, both governed by the same process. This process could be reaction time, which could control both the evolution of  $\delta^{13}\text{C}_{\text{DIC}}$  values through Rayleigh distillation during ureolysis (see Appendix B6) and the evolution of  $\delta^{18}\text{O}_{\text{DIC}}$  values through oxygen isotope equilibration between DIC and water. To summarize, the progressive  $\delta^{18}\text{O}_{\text{CaCO}_3}$  increase observed in the course of the experiment may be due to oxygen isotope equilibration between DIC and water and/or to kinetic isotope fractionation during ureolysis.

In conclusion, the initial  $\delta^{18}\text{O}_{\text{CaCO}_3}$  offset from isotopic equilibrium between water, solid carbonates and DIC is likely to result from a combination of hypothesis (4) and (5), which are directly or indirectly linked to the metabolic production of DIC by ureolysis. If ureolysis produces  $\text{H}_2\text{CO}_3$  instead of  $\text{CO}_{2(\text{aq})}$ , then all the oxygen isotope disequilibrium must be attributed to the ureolysis reaction.

#### 4.4. Implications for the interpretation of $\delta^{18}\text{O}$ values in microbially induced carbonates

Our results demonstrate that bacterial activity can produce calcium carbonates with an oxygen isotopic composition in disequilibrium with the ambient water. In our experiments, the disequilibrium gave  $1000\ln\alpha_{\text{CaCO}_3\text{-H}_2\text{O}}$  values 24.7‰ smaller than equilibrium and result from a combination of  $\text{H}_2\text{CO}_3$  or  $\text{CO}_{2(\text{aq})}$  produced by ureolysis with a metabolic isotopic signature and kinetic isotope effect during potential  $\text{CO}_{2(\text{aq})}$  hydration and hydroxylation. For disequilibrium to be

recorded in microbially mediated carbonates, favorable conditions are required. Precipitation should occur in a confined space favoring the accumulation of metabolic DIC and limiting its dilution in the environmental DIC. Additionally, the oxygen isotope equilibration of metabolic DIC with water must not reach completion before carbonate precipitation. This would be favored by a short residence time of metabolic DIC in water before carbonate precipitation, facilitated by a relatively high local pH (as stated previously, the rate of isotope equilibration between DIC and water takes around 44 hours at pH 9 and less than one hour at pH 7 (Zeebe and Wolf-Gladrow, 2001; Watkins et al., 2013)). Additionally, hydroxylation of CO<sub>2</sub> is favored over hydration at high pH, further enhancing disequilibrium DIC formation as hydroxylation presents the strongest oxygen isotope effect.

Microbially mediated carbonates showing disequilibrium isotopic compositions for oxygen have already been identified and it was proposed that disequilibrium may result from metabolic activity (Coleman and Raiswell, 1995; Sass et al., 1991). Geological evidence is nonetheless still scarce, as carbonate exclusively precipitated by microbial activity are difficult to identify and isolate from other types of carbonates. In addition, the  $\delta^{18}\text{O}$  value of the water in which microbial carbonates precipitated is often poorly constrained or even unknown, as in the cases of some ancient lakes or ground waters. Because a small change in water  $\delta^{18}\text{O}$  value causes large change in isotopically-predicted temperatures, the microbial record is rarely chosen for paleoenvironmental studies (Andrews et al., 1997). However, microbial carbonates were shown to be important in certain geological periods (e.g., Leinfelder et al. (1993) for the Jurassic period) and for some particular settings or carbonate types (i.e., Cacchio et al. (2004) for cave carbonate and Wacey et al. (2007) for dolomite formation). Moreover, microbial carbonates sometimes are the only carbonates available, in particular in the subsurface and during the Precambrian.

Concretions produced during diagenetic processes are the most likely carbonated materials to record oxygen isotopic disequilibrium due to the involvement of microbes in their formation. Furthermore, their precipitation occurs in the relatively confined porosity of sediments, where fluid

circulations are strongly reduced compared to free water. pH is locally controlled and *de facto* high enough to allow rapid carbonate precipitation. A few authors have already suggested that a DIC of metabolic origin could be an explanation for the combined disequilibrium  $\delta^{18}\text{O}$  and  $\delta^{13}\text{C}$  values found in several carbonated cements and concretions associated with sediments. The fractionation mechanism invoked to account for these disequilibrium isotopic values was the incorporation of microbially produced  $\text{HCO}_3^-$  in the precipitating carbonate (Coleman and Raiswell, 1995; Sass et al., 1991; Nielsen et al., 1998; Mortimer and Coleman 1997; DeCraen et al., 1999; Bojanowski and Clarkson, 2012). Our experimental results lend a strong support to the so far poorly supported idea that, due to their metabolic activity, microbes can precipitate carbonates with  $\delta^{18}\text{O}$  values in disequilibrium with water. This does not mean however that this is the case for all microbial carbonates. For example, carbonate precipitating in close contact to open waters relatively rich in ambient DIC, such as in microbialites (among which are the emblematic stromatolites), should be less prone to record oxygen isotope disequilibria. As an example, it has been shown that metabolic effects could only be imprinted below the stromatolites surface, in the finest carbonate grains, whereas the carbonate crust in contact with water was found to form at oxygen isotope equilibrium (Andres et al., 2006). Moreover, compared to other biogenic carbonates, microbial carbonates are often composed of small and poorly crystallized grains. They are thus more prone to dissolution-reprecipitation with a consequent loss of the original disequilibrium oxygen isotope signature. Yet, the possibility that the oxygen isotope signatures of microbial carbonates may be offset from equilibrium with water should receive more consideration, in particular in diagenetic cements and sedimentary concretions.

## 5. CONCLUSIONS

We presented here an experimental study on the oxygen isotope systematics of carbonate precipitation induced by bacterial ureolysis. Based on the results of two experiments conducted with

a model carbonatogenic strain, respectively in the presence and in the absence of CA, we showed that the oxygen isotope composition of solid carbonates was controlled by the microbial metabolic activity. While, in the absence of CA, carbonates precipitated in strong oxygen isotope disequilibrium with water, this equilibrium was quickly reached in the presence of CA. The maximum offset from equilibrium observed in the carbonates precipitated without CA was  $-24.7\text{‰}$ , while carbonates eventually precipitated at equilibrium in the presence of CA. The fact that CA promoted oxygen isotope equilibrium between carbonate and water implies that the cause for the disequilibrium in the absence of CA was the disequilibrium between DIC and water rather than the disequilibrium between solid carbonates and DIC. This disequilibrium resulted from the combination of a source effect (i.e.,  $\text{H}_2\text{CO}_3$  or  $\text{CO}_{2(\text{aq})}$  generated by ureolysis) with a kinetic effect associated with hydroxylation/hydration of this  $\text{CO}_{2(\text{aq})}$ , the respective contribution of which remains unknown.

This finding gives credit to the long-standing but poorly supported hypothesis that in some cases oxygen disequilibrium recorded in microbial carbonate may, like in eukaryotes, result from the incorporation of variable proportions of metabolic  $\text{CO}_2$  within the solid carbonate. It is possible (but not demonstrated yet) that this metabolic  $\text{CO}_2$ , initially out equilibrium with water, may undergo further  $^{18}\text{O}$  depletion through a kinetic effect associated with its conversion into bicarbonate or carbonic acid during hydroxylation or hydration reactions. Our experiment also suggests the hypothesis that CA activity in precipitation sites could lower or suppress the vital effects (i.e. oxygen isotope disequilibrium of carbonates with respect to water) in numerous species of skeleton-forming eukaryotes (Weiner and Dove, 2003).

The main result of this study is that disequilibrium oxygen isotope ratios, which are widely recorded in carbonate mineralizing eukaryotes, can also occur in the case of microbially-induced carbonate precipitation. Such disequilibrium oxygen isotope ratios might complicate the interpretations of the  $\delta^{18}\text{O}$  signatures of microbial carbonates in terms of reconstructions of paleotemperature or  $\delta^{18}\text{O}$  value of water, especially in subsurface environments where diagenesis

occurs, but they also might offer a new opportunity to identify biogenic carbonates in the subsurface.

## ACKNOWLEDGEMENTS

We gratefully acknowledge the support of ADEME, Schlumberger and Total in this project and their permission to publish this paper. However, the views expressed here are those of the authors who are solely responsible for any errors. We also gratefully acknowledge Pierre Agrinier for his advices, proofreading and his recommendations for model and error calculations. We are grateful to our anonymous reviewers for their valuable comments. This is IPGP contribution n°3801.

## REFERENCES

- Adkins J. F., Boyle E. A., Curry W. B. and Lutringer A. (2003) Stable isotopes in deep-sea corals and a new mechanism for “vital effects”. *Geochim. Cosmochim. Acta* **67**, 1129–1143.
- Aloisi G., Gloter A., Krüger M., Wallmann K., Guyot F. and Zuddas P. (2006) Nucleation of calcium carbonate on bacterial nanoglobules. *Geology* **34**, 1017–1020.
- Andres M. S., Sumner D. Y., Reid R. P., and Swart, P. K. (2006) Isotopic fingerprints of microbial respiration in aragonite from Bahamian stromatolites. *Geology* **34**, 973–976.
- Andrews R. K., Blakeley R. L. and Zerner B. (1984) Urea and urease. *Adv. Inorg. Biochem.* **6**, 245–283.
- Andrews J. E., Riding R. and Dennis P. F. (1997) The stable isotope record of environmental and climatic signals in modern terrestrial microbial carbonates from Europe. *Palaeogeogr. Palaeoclimatol. Palaeoecol.* **129**, 171–189.

- Arashisar Ş., Hisar O., Yanık T. and Aras S. M. (2004) Inhibitory effects of ammonia and urea on gill carbonic anhydrase enzyme activity of rainbow trout *Oncorhynchus mykiss*. *Environ. Toxicol. Pharmacol.* **17**, 125–128.
- Azaroual M., Fouillac C. and Matray J. M. (1997) Solubility of silica polymorphs in electrolyte solution, II. Activity of aqueous silica and solid silica polymorphs in deep solutions from the sedimentary Paris basin. *Chem. Geol.* **140**, 167–179.
- Baskar S., Baskar R., Mauclaire L. and McKenzie J. A. (2006) Microbially induced calcite precipitation in culture experiments: Possible origin for stalactites in Sahastradhara caves, Dehradun. *India. Curr. Sci.* **90**, 58–64.
- Beck W. C., Grossman E. L. and Morse J. W. (2005) Experimental studies of oxygen isotope fractionation in the carbonic acid system at 15, 25 and 40°C. *Geochim. Cosmochim. Acta* **69**, 3493–3503.
- Bemis B. E., Spero H. J., Bijma J. and Lea D.W. (1998) Reevaluation of the oxygen isotopic composition of planktonic foraminifera: Experimental results and revised paleotemperature equations. *Paleoceanography* **13**, 150–160.
- Bojanowski M. J. and Clarkson E. N. (2012) Origin of siderite concretions in microenvironments of methanogenesis developed in a sulfate reduction zone: an exception or a rule? *J. Sediment. Res.* **82**, 585–598.
- Burns S. J. (1998) Can diagenetic precipitation of carbonate nodules affect pore-water oxygen isotope ratios? *J. Sediment. Res.* **68**, 100–103.
- Cacchio P., Contento R., Ercole C., Cappuccio G., Martinez M. P. and Lepidi A. (2004) Involvement of microorganisms in the formation of carbonate speleothems in the Cervo Cave (L'Aquila-Italy). *Geomicrobiol. J.* **21**, 497–509.
- Castanier S., Le Métayer–Levrel G. and Perthuisot J.–P. (1999) Ca–carbonates precipitation and limestone genesis – the microbiogeologist point of view. *Sediment. Geol.* **126**, 9–23.

- Cerling T. E. and Quade J. (1993) Stable carbon and oxygen isotopes in soil carbonates. In *Climate Change in Continental Isotopic Records*, vol. 78 (eds. P. K. Swart, K. C. Lohmann, J. Mckenzie and S. Savin), AGU Geophysical Monograph Series, pp. 217–231.
- Chacko T. and Deines P. (2008) Theoretical calculation of oxygen isotope fractionation factors in carbonate systems. *Geochim. Cosmochim. Acta* **72**, 3642–3660.
- Chafetz H. S. and Lawrence J. R. (1994) Stable isotopic variability within modern travertines. *Geogr. Phys. Quatern.* **48**, 257–273.
- Clark I. D., Fontes J.–C. and Fritz P. (1992) Stable isotope disequilibria in travertine from high pH waters: Laboratory investigations and field observations from Oman. *Geochim. Cosmochim. Acta* **56**, 2041–2050.
- Coleman M. L. and Raiswell R. (1995) Source of carbonate and origin of zonation in pyritiferous carbonate concretions; evaluation of a dynamic model. *Am. J. Sci.* **295**, 282–308.
- Coplen T. B., Kendall C. and Hopple J. (1983) Intercomparison of stable isotope reference samples. *Nature* **302**, 236–238.
- Coplen T. B. (2007) Calibration of the calcite–water oxygen–isotope geothermometer at Devils Hole, Nevada, a natural laboratory. *Geochim. Cosmochim. Acta* **71**, 3948–3957.
- Craig H. (1953) The geochemistry of the stable carbon isotopes. *Geochim. Cosmochim. Acta* **3**, 53–92.
- De Craen M., Swennen R., Keppens E. M., Macaulay C. I. and Kiriakoulakis K. (1999) Bacterially mediated formation of carbonate concretions in the Oligocene Boom Clay of northern Belgium. *J. Sediment Res.* **69**, 1098–1106.
- Dietzel M., Tang J., Leis A. and Koehler S. J. (2009) Oxygen isotopic fractionation during inorganic calcite precipitation – Effects of temperature, precipitation rate and pH. *Chem. Geol.* **268**, 107–115.
- Dupraz C., Reid R. P., Braissant O., Decho A. W., Norman R. S., and Visscher P. T. (2009) Processes of carbonate precipitation in modern microbial mats. *Earth Sci. Rev.* **96**, 141–162.

- Dupraz S., Parmentier M., Ménez B. and Guyot F. (2009a) Experimental and numerical modelling of bacterially induced pH increase and calcite precipitation in saline aquifers. *Chem. Geol.* **265**, 44–53.
- Dupraz S., Ménez B., Gouze P., Leprovost R., Bénézech P., Pokrovsky O. S. and Guyot F. (2009b) Experimental approach of CO<sub>2</sub> biomineralization in deep saline aquifers. *Chem. Geol.* **265**, 54–62.
- Epstein S., Buchsbaum R., Lowenstam H. A. and Urey H. C. (1953) Revised carbonate-water isotopic temperature scale. *Geol. Soc. Am. Bull.* **64**, 1315–1326.
- Erez J. (1978) Vital effect on stable-isotope composition seen in foraminifera and coral skeletons. *Nature* **273**, 199–202.
- Erez J. and Luz B. (1983) Experimental paleotemperature equation for planktonic foraminifera. *Geochim. Cosmochim. Acta* **47**, 1025–1031.
- Ferris F. G., Phoenix V., Fujita Y. and Smith R. W. (2003) Kinetics of calcite precipitation induced by ureolytic bacteria at 10 to 20°C in artificial groundwater. *Geochim. Cosmochim. Acta* **67**, 1701–1722.
- Fujita Y., Taylor J. L., Gresham T. L. T., Delwiche M. E., Colwell F. S., McLing T. L., Petzke L. M. and Smith R. W. (2008) Stimulation of microbial urea hydrolysis in groundwater to enhance calcite precipitation. *Environ. Sci. Technol.* **42**, 3025–3032.
- Furla P., Galgani I., Durand I. and Allemand D. (2000) Sources and mechanisms of inorganic carbon transport for coral calcification and photosynthesis. *J. Exp. Biol.* **203**, 3445–3457.
- Gabitov R. I., Watson E. B. and Sadekov A. (2012) Oxygen isotope fractionation between calcite and fluid as a function of growth rate and temperature: An in situ study. *Chem. Geol.* **306**, 92–102.
- Gradzinski M. (2003) Bacterial influence on speleothem oxygen isotope composition: An example based on cave pisoids from Perlová Cave (Slovakia). *Geol. Carpath.* **54**, 199–204.

- Green M. and Taube H. (1963) The mechanism of base hydrolysis of substituted pentaamminecobalt (III) complexes. *Inorg. Chem.* **2**, 948–950.
- Grossman E. L. (1987) Stable isotopes in modern benthic foraminifera: a study of vital effect. *J. Foramin. Res.* **17**, 48–61.
- Grotzinger, J. P. (1989) Facies and evolution of Precambrian carbonate depositional systems: emergence of the modern platform archetype. In *Controls on Carbonate Platform and Basin Development*, vol. 44 (eds. P. D. Crevello, J. L. Wilson, J. F. Sarg, J. F. Read) Soc. Econ. Paleont. Mineral. Special Publication, Tulsa, pp. 79–106.
- Guido A., Jacob J., Gautret P., Laggoun-Défarge F., Mastandrea A. and Russo F. (2007) Molecular fossils and other organic markers as palaeoenvironmental indicators of the Messinian Calcare di Base Formation: normal *versus* stressed marine deposition (Rossano Basin, northern Calabria, Italy). *Palaeogeogr. Palaeoclimatol.* **255**, 265–283.
- Ishimura T., Tsunogai U., Hasegawa S., Nakagawa F., Oi T., Kitazato H. and Toyofuku T. (2012) Variation in stable carbon and oxygen isotopes of individual benthic foraminifera: tracers for quantifying the vital effect. *Biogeosciences* **9**, 4353–4367.
- Jahns T. (1996) Ammonium/Urea-dependent generation of a proton electrochemical potential and synthesis of ATP in *Bacillus pasteurii*. *J. Bacteriol.* **178**, 403–409.
- Jiménez-López C., Caballero E., Huertas F. J. and Romanek C. S. (2001) Chemical, mineralogical and isotope behavior, and phase transformation during the precipitation of calcium carbonate minerals from intermediate ionic solution at 25°C. *Geochim. Cosmochim. Acta* **65**, 3219–3231.
- Johnson C. M., Ludois J. M., Beard B. L., Beukes N. J. and Heimann A. (2013) Iron formation carbonates: Paleooceanographic proxy or recorder of microbial diagenesis? *Geology* **41**, 1147–1150.
- Kim S. T. and O'Neil J. R. (1997) Equilibrium and nonequilibrium oxygen isotope effects in synthetic carbonates. *Geochim. Cosmochim. Acta* **61**, 3461–3475.

- Kim S.-T., Gebbinck C. K., Mucci A. and Coplen T. B. (2014) Oxygen isotopes systematics in the aragonite-CO<sub>2</sub>-H<sub>2</sub>O-NaCl system up to 0.7 mol/kg ionic strength at 25°C. *Geochim. Cosmochim. Acta* **137**, 147–158.
- Kishimoto S., Shimura R., Kamijo T. (2008) MHI Proprietary process for reducing CO<sub>2</sub> emission and increasing urea Production. Nitrogen + Syngas 2008 International Conference and Exhibition, Moscow.
- Krajewska B. (2009) Ureases I. Functional, catalytic and kinetic properties: A review. *J. Mol. Catal. B: Enzym.* **59**, 9–21.
- Krebs H. A. and Roughton F. J. W. (1948) Carbonic anhydrase as a tool in studying the mechanism of reactions involving H<sub>2</sub>CO<sub>3</sub>, CO<sub>2</sub> or HCO<sub>3</sub><sup>-</sup>. *Biochem. J.* **43**, 550–555.
- Leinfelder R. R., Nose M., Schmid D. U. and Werner W. (1993) Microbial crusts of the Late Jurassic: composition, palaeoecological significance and importance in reef construction. *Facies* **29**, 195–229.
- Létolle R., Gegout P., Gaveau B. and Moranville-Regourd M. (1990) Fractionnement isotopique de l'oxygène dans la précipitation des carbonates à pH très élevés. *CR. Acad. Sci. II.* **310**, 547–552.
- Lindskog S. (1997) Structure and mechanism of carbonic anhydrase. *Pharmacol. Therapeut.* **74**, 1–20.
- Lindskog S. and Coleman J. E. (1973) The catalytic mechanism of carbonic anhydrase. *P. Natl. Acad. Sci. USA* **70**, 2505–2508.
- Matsuzaki Y., Yamada H., Chowdhury F. A., Higashii T., Kazama S. and Onoda M. (2013) Ab initio study of CO<sub>2</sub> capture mechanisms in monoethanolamine aqueous solution: reaction pathways from carbamate to bicarbonate. *Energy Procedia* **37**, 400–406.
- Mavromatis V., Bundeleva I. A., Shirokova L. S., Millo C., Pokrovsky O. S., Bénézech P., Ader M. and Oelkers E. H. (2015) The continuous re-equilibration of carbon isotope compositions of hydrous Mg carbonates in the presence of cyanobacteria. *Chem. Geol.* **404**, 41–51.

- McConnaughey T. (1989a)  $^{13}\text{C}$  and  $^{18}\text{O}$  isotopic disequilibrium in biological carbonates: I. Patterns. *Geochim. Cosmochim. Acta* **53**, 151–162.
- McConnaughey T. (1989b)  $^{13}\text{C}$  and  $^{18}\text{O}$  isotopic disequilibrium in biological carbonates: II. In vitro simulation of kinetic isotope effects. *Geochim. Cosmochim. Acta* **53**, 163–171.
- McConnaughey T. (2003) Sub-equilibrium oxygen-18 and carbon-13 levels in biological carbonates: carbonate and kinetic models. *Coral Reefs* **22**, 316–327.
- McConnaughey T. A., Burdett J., Whelan J. F. and Paull C. K. (1997) Carbon isotopes in biological carbonates: respiration and photosynthesis. *Geochim. Cosmochim. Acta* **61**, 611–622.
- McCrea J. M. (1950) On the isotopic chemistry of carbonates and a paleotemperature scale. *J. Chem. Phys.* **18**, 849–857.
- Millo C., Dupraz S., Ader M., Guyot F., Thaler C., Foy E. and Ménez B. (2012). Carbon isotope fractionation during calcium carbonate precipitation induced by ureolytic bacteria. *Geochim. Cosmochim. Acta* **98**, 107–124.
- Mitchell A. C. and Ferris F. G. (2005) The coprecipitation of Sr into calcite precipitates induced by bacterial ureolysis in artificial groundwater: Temperature and kinetic dependence. *Geochim. Cosmochim. Acta* **69**, 4199–4210.
- Mobley H. L. T. and Hausinger R. P. (1989) Microbial ureases significance, regulation and molecular characterization. *Microbiol. Rev.* **53**, 85–108.
- Mook W. G. (1971) Paleotemperatures and chlorinities from stable carbon and oxygen isotopes in shell carbonate. *Palaeogeogr. Palaeoclimatol. Palaeoecol.* **9**, 245–263.
- Mortimer R. J. G. and Coleman M. L. (1997) Microbial influence on the oxygen isotopic composition of diagenetic siderite. *Geochim. Cosmochim. Acta* **61**, 1705–1711.
- Nielsen T. H., Bonde T. A. and Sorensen J. (1998) Significance of microbial urea turnover in N cycling of three Danish agricultural soils. *FEMS Microbiol. Ecol.* **25**, 147–157.
- O'Neil J. R., Clayton R. N. and Mayeda T. K. (1969) Oxygen isotope fractionation in divalent metal carbonates. *J. Chem. Phys.* **51**, 5547–58

- Pazdur A., Pazdur M. F., Starkel L. and Szulc J. (1988) Stable isotopes of Holocene calcareous tufa in southern Poland as paleoclimatic indicators. *Quat. Res.* **30**, 177–189.
- Riding R. (2000) Microbial carbonates: The geological record of calcified bacterial- algal mats and biofilms. *Sedimentology* **47**, 179–214.
- Rollion-Bard C., Chaussidon M. and France-Lanord C. (2003) pH control on oxygen isotopic composition of symbiotic corals. *Earth Planet. Sc. Lett.* **215**, 275–288.
- Romanek C. S., Grossman E. L. and Morse J. W. (1992) Carbon isotope fractionation in synthetic aragonite and calcite: Effects of temperature and precipitation rate. *Geochim. Cosmochim. Acta* **56**, 419–430.
- Rusznayk A., Akob D. M., Nietzsche S., Eusterhues K., Totsche K. U., Neu T. R. and Küsel K. (2012) Calcite biomineralization by bacterial isolates from the recently discovered pristine karstic Herrenberg cave. *Appl. Environ. Microbiol.* **78**, 1157–1167.
- Sass E., Bein A. and Almogi-Labin A. (1991) Oxygen-isotope composition of diagenetic calcite in organic-rich rocks: evidence for  $^{18}\text{O}$  depletion in marine anaerobic pore water. *Geology* **19**, 839–842.
- Smith D. G. E., Russel W. C., Ingledew W. J. and Thirkell D. (1993) Hydrolysis of urea by *Ureaplasma urealyticum* generates a transmembrane potential with resultant ATP synthesis. *J. Bacteriol.* **175**, 3253–3258.
- Spero H. J., Bijma J., Lea D. W. and Bemis B. E. (1997) Effect of seawater carbonate concentration on foraminiferal carbon and oxygen isotopes. *Nature* **390**, 497–500.
- Swensen B. and Bakken L. R. (1998) Nitrification potential and urease activity in a mineral subsoil. *Soil Biol. Biochem.* **30**, 1333–1341.
- Tang J., Koehler S. J. and Dietzel M. (2008)  $\text{Sr}^{2+}/\text{Ca}^{2+}$  and  $^{44}\text{Ca}/^{40}\text{Ca}$  fractionation during inorganic calcite formation: I. Sr incorporation. *Geochim. Cosmochim. Acta* **72**, 3718–3732.

- Tarutani T., Clayton R.N. and Mayeda T.K. (1969) Effect of polymorphism and magnesium substitution on oxygen isotope fractionation between carbonate and water. *Geochim. Cosmochim. Acta* **33**, 987–996.
- Thiagarajan N., Adkins J. and Eiler J. (2011) Carbonate clumped isotope thermometry of deep-sea corals and implications for vital effects. *Geochim. Cosmochim. Acta* **75**, 4416–4425.
- Tobler D. J., Cuthbert M. O., Greswell R. B., Riley M. S., Renshaw J. C., Handley–Sidhu S. and Phoenix V. R. (2011) Comparison of rates of ureolysis between *Sporosarcina pasteurii* and an indigenous groundwater community under conditions required to precipitate large volumes of calcite. *Geochim. Cosmochim. Acta* **75**, 3290–3301.
- Uchikawa J. and Zeebe R. E. (2012) The effect of carbonic anhydrase on the kinetics and equilibrium of the oxygen isotope exchange in the CO<sub>2</sub>–H<sub>2</sub>O system: Implications for δ<sup>18</sup>O vital effects in biogenic carbonates. *Geochim. Cosmochim. Acta*, **95**, 15–34.
- Urey H. C. (1947) The thermodynamic properties of isotopic substances. *J Chem. Soc.*, 562–581.
- Urey H. C., Lowenstam H. A., Epstein S. and McKinney C. R. (1951) Measurement of paleotemperatures and temperatures of the Upper Cretaceous of England, Denmark, and the southeastern United States. *Geol. Soc. Am. Bull.* **62**, 399–416.
- Uzdowski E., Michaelis J., Bottcher M. E. and Hoefs J. (1991) Factors for the oxygen isotope equilibrium fractionation between aqueous and gaseous CO<sub>2</sub>, carbonic-acid, bicarbonate, carbonate and water (19°C). *Z. Phys. Chem.* **170**, 237–249.
- Uzdowski E. and Hoefs J. (1993) Oxygen isotope exchange between carbonic acid, bicarbonate, carbonate, and water: a re-examination of the data of McCrea (1950) and an expression for the overall partitioning of oxygen isotopes between the carbonate species and water. *Geochim. Cosmochim. Acta* **57**, 3815–3818.
- Van der Lee J. (1998) Thermodynamic and mathematical concepts of CHESS<sup>®</sup>. Technical Report Nr. LHM/RD/98/39 CIG–Ecole des Mines de Paris, Fontainebleau, France, pp 99.

- Van Lith Y., Warthmann R., Vasconcelos C. and McKenzie J. A. (2003) Microbial fossilization in carbonate sediments: a result of the bacterial surface involvement in dolomite precipitation. *Sedimentology* **50**, 237–245.
- Vasconcelos C., McKenzie J.A., Warthmann R. and Bernasconi S. (2005) Calibration of the  $\delta^{18}\text{O}$  paleothermometer for dolomite precipitated in microbial cultures and natural environments. *Geology* **33**, 317–320.
- Wacey D., Wright D. T. and Boyce A. J. (2007) A stable isotope study of microbial dolomite formation in the Coorong Region, South Australia. *Chem. Geol.* **244**, 155–174.
- Watkins J. M., Nielsen L. C., Ryerson F. J. and DePaolo D. J. (2013) The influence of kinetics on the oxygen isotope composition of calcium carbonate. *Earth Planet. Sc. Lett.* **375**, 349–360.
- Weiner S. and Dove P. M. (2003) An overview of biomineralization processes and the problem of the vital effect. *Rev. Mineral. Geochem.* **54**, 1–29.
- Wilbur K. and Anderson N. (1948) Electrometric and colorimetric determination of carbonic anhydrase. *J. Biol. Chem.* **176**, 147–154.
- Zeebe R. E. (1999) An explanation of the effect of seawater carbonate concentration on foraminiferal oxygen isotopes. *Geochim. Cosmochim. Acta* **63**, 2001–2007.
- Zeebe R. E. (2007) An expression for the overall oxygen isotope fractionation between the sum of dissolved inorganic carbon and water. *Geochem. Geophys. Geosyst.* **8**, Q09002, doi:10.1029/2007GC001663.
- Zeebe R. E. and Wolf-Gladrow D. (2001) *CO<sub>2</sub> in seawater: Equilibrium, kinetics, isotopes*. Elsevier oceanography series **65**, the Netherlands, pp 346.
- Ziveri P., Stoll H., Probert I., Klaas C., Geisen M., Ganssen G. and Young J. (2003) Stable isotope ‘vital effects’ in coccolith calcite. *Earth Planet. Sci. Lett.* **210**, 137–149.

## Appendix A. Saturation index calculations

The evolutions of the saturation indexes ( $\Omega$ ) (Eq. A1) of calcite, aragonite and vaterite in the course of the experiment, both in the presence and in the absence of CA, are displayed in Fig. A1. Saturations indexes were calculated as follows:

$$\Omega = \frac{\{Ca^{2+}\}\{CO_3^{2-}\}}{K_{sp}} \quad (A1)$$

where  $\{Ca^{2+}\}$  and  $\{CO_3^{2-}\}$  are the activities of dissolved  $Ca^{2+}$  and  $CO_3^{2-}$  given by a truncated Davies model.  $K_{sp}$  is the solubility product of  $CaCO_3$  at the experimental temperature of 30°C and was calculated for each of the three  $CaCO_3$  polymorphs (calcite, vaterite and aragonite). The log of the formation constant of each polymorph, namely  $K_{calcite}$ ,  $K_{vaterite}$  and  $K_{aragonite}$ , were those of the JCHESS<sup>®</sup> default database updated with  $\log K_{vaterite}$  after Plummer and Busenberg (1982) ( $\log K_{calcite} = -8.51$ ,  $\log K_{aragonite} = -8.37$ ,  $\log K_{vaterite} = -7.96$ ). Saturation indexes evolution indicated that in both experiments (with ou without AC) calcite was systematically the most thermodynamically favourable calcium carbonate polymorph, followed by aragonite and vaterite.

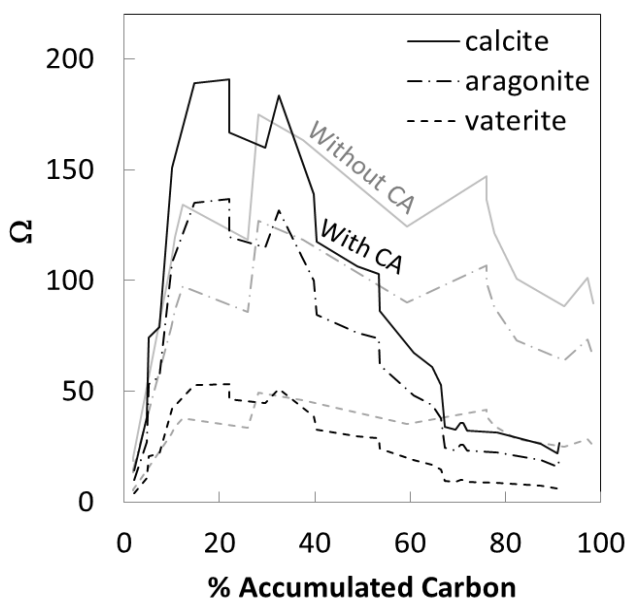


**Figure A1.** Saturation index ( $\Omega$ ) of the solution with respect to calcite, aragonite and vaterite during the experiments with (in black) or without (in gray) carbonic anhydrase (calculated using JCHESS<sup>®</sup> and plotted versus the percentage of Accumulated Carbon).

**Table A1.** Temporal evolution of DIC speciation and saturation index calculated using the geochemical code JCHESS<sup>®</sup> for the experiment with AC. The reader is referred to Millo et al. (2012) for the data associated with the experiment without AC.

Reaction time (min)	HCO <sub>3</sub> <sup>-</sup> (%)	CO <sub>3</sub> <sup>2-</sup> (%)	CO <sub>2(aq)</sub> (%)	Ω (calcite)	Ω (vaterite)	Ω (aragonite)
20	72.7	27.1	0.2	14.0	3.9	10.0
27	65.3	34.6	0.1	38.0	10.6	27.2
40	59.1	40.8	0.1	74.3	20.7	53.3
50	58.0	42.0	0.1	78.9	22.0	56.6
69	57.0	43.0	0.1	150.7	42.0	108.1
83	56.7	43.3	0.1	188.8	52.6	135.2
94	59.7	40.2	0.1	190.5	53.2	136.8
116	68.3	31.6	0.1	166.7	46.5	119.7
127	71.6	28.2	0.2	160.0	44.6	114.8
142	68.5	31.4	0.1	183.2	51.2	131.5
156	74.2	25.6	0.2	139.0	38.8	99.8
186	79.7	20.1	0.2	117.5	32.8	84.3
219	80.8	18.9	0.3	106.2	29.6	76.2
247	83.0	16.7	0.3	102.8	28.7	73.8
275	82.4	17.3	0.2	86.3	24.1	61.8
303	85.3	14.4	0.3	67.3	18.8	48.2
334	86.8	12.9	0.3	60.7	17.0	43.6
369	86.8	12.9	0.3	52.7	14.7	37.8
394	91.6	7.9	0.5	34.0	9.5	24.3
404	90.5	9.1	0.4	32.5	9.1	23.3
405	90.3	9.3	0.4	35.8	10.0	25.6
424	90.5	9.1	0.4	35.8	10.0	25.7
454	90.4	9.2	0.4	32.3	9.0	23.2
481	90.2	9.4	0.3	31.3	8.7	22.4
24 h	89.3	10.5	0.3	26.1	7.3	18.7
24 h	89.3	10.4	0.3	21.9	6.1	15.7
24 h	89.1	10.7	0.3	26.4	7.4	19.0

### Appendix A references

Millo C., Dupraz S., Ader M., Guyot F., Thaler C., Foy E. and Ménez B. (2012). Carbon isotope fractionation during calcium carbonate precipitation induced by ureolytic bacteria. *Geochim. Cosmochim. Acta* **98**, 107–124.

Plummer L. N. and Busenberg E. (1982) The solubilities of calcite, aragonite and vaterite in CO<sub>2</sub>-H<sub>2</sub>O solutions between 0 and 90°C, and an evaluation of the aqueous model for the system CaCO<sub>3</sub>-CO<sub>2</sub>-H<sub>2</sub>O. *Geochim. Cosmochim. Acta* **46**, 1011–1040.

## Appendix B. Isotopic measurements and carbon systematics

### B1. $\delta^{13}\text{C}_{\text{DIC}}$ and $\delta^{18}\text{O}_{\text{H}_2\text{O}}$ measurements

Aliquots of 2 mL of the experimental solution were collected for isotopic analysis at each sampling event. For  $\delta^{18}\text{O}_{\text{H}_2\text{O}}$  analyses, a 1 mL aliquot was injected in an Exetainer<sup>®</sup> vial filled with a mixture of 99.7% helium and 0.3%  $\text{CO}_2$  according to the water- $\text{CO}_2$  equilibration method (Horita and Kendall, 2004). The remaining 1 mL was injected in a separate Exetainer<sup>®</sup> vial loaded with 0.2 mL of 100%  $\text{H}_3\text{PO}_4$  and filled with helium for  $\delta^{13}\text{C}_{\text{DIC}}$  values analyses. Isotope equilibration between gaseous and aqueous  $\text{CO}_2$  was established for both by vial agitation overnight.

Isotope analyses were performed with two gas chromatography isotope ratio mass spectrometers (GC-IRMS) running under continuous helium flow, namely AP 2003 (Analytical Precision 2003, GV Instruments) or Gas Bench coupled to a Delta XP Thermo Finnigan. Raw  $\delta^{18}\text{O}$  and  $\delta^{13}\text{C}$  values (obtained by averaging four consecutive measurements) were corrected for non-linearity according to standard procedures (e.g., Assayag et al., 2006). The analytical uncertainty on  $\delta^{18}\text{O}_{\text{H}_2\text{O}}$  and  $\delta^{13}\text{C}_{\text{DIC}}$  values was  $\pm 0.1 \text{ ‰}$  ( $1\sigma$ ).

The concentration of DIC, linked to the molar quantity of DIC ( $C_{\text{DIC}}$ ) produced in each assay, was inferred from the linear relationship between the molar quantity of sample and the intensity of the mass 44 peak provided by the mass spectrometer (i.e., the  $^{12}\text{C}^{16}\text{O}_2^+$  ion currents, henceforth referred to as  $I_{44}$ ). This linear relationship was established by repeated analyses of internal laboratory carbonate standards (100% calcite), run with different concentrations. The uncertainty in the  $C_{\text{DIC}}$  quantification was  $\pm 5\%$  of the measured values ( $1\sigma$ ).

### B2. $\delta^{13}\text{C}$ and $\delta^{18}\text{O}$ analysis of calcium carbonate precipitates

Carbon and oxygen isotope compositions of calcium carbonate precipitates ( $\delta^{18}\text{O}_{\text{CaCO}_3}$  and  $\delta^{13}\text{C}_{\text{CaCO}_3}$ ) were measured using the AP 2003 GC-IRMS. Aliquots of 0.6 to 3.5 mg of precipitates along with calcium carbonate standards were loaded in Exetainer<sup>®</sup> vials, flushed with ultra-pure helium gas (at a pressure of 2.5 bar) and digested at ambient temperature in an excess of 100%  $\text{H}_3\text{PO}_4$  injected through the Exetainer<sup>®</sup> rubber septa (refer to Assayag et al. (2006) for further details). Raw  $\delta^{18}\text{O}_{\text{CaCO}_3}$  and  $\delta^{13}\text{C}_{\text{CaCO}_3}$  values were measured after 15 to 20 hours acid digestion, corrected for instrumental non-linearity and converted to the V-SMOW or V-PDB scale as

described in Assayag et al. (2006). The analytical precision for both  $\delta^{18}\text{O}_{\text{CaCO}_3}$  and  $\delta^{13}\text{C}_{\text{CaCO}_3}$  estimates was  $\pm 0.1\text{‰}$  ( $1\sigma$ ).

### B3. Blank correction for DIC and Accumulated Carbon

Pre-existing DIC in AGW and bacterial suspension prior to inoculation was identified and is hereafter referred to as blank DIC. The presence of blank DIC in the initial solutions probably results from the dissolution of atmospheric  $\text{CO}_{2(\text{g})}$  in solution prior to inoculation and/or to the release of metabolic  $\text{CO}_{2(\text{aq})}$  in the bacterial suspension prior to ureolysis in AGW.

Carbon isotope analyses of the blank DIC in 12 mL of pure AGW and 12 mL of pure *S. pasteurii* inoculum suspended in UPW at  $\text{OD}_{600} = 0.100$ , respectively yielded the following results:

(a) AGW:  $C_{\text{DIC}} = 167 \mu\text{mol/L}$ ;  $\delta^{13}\text{C}_{\text{DIC}} = -35.0\text{‰}$ .

(b) *S. pasteurii* inoculum:  $C_{\text{DIC}} = 156 \mu\text{mol/L}$ ;  $\delta^{13}\text{C}_{\text{DIC}} = -32.0\text{‰}$ .

Mass and isotopic balance of the contributions (a) and (b) calculated for a mix of 6 mL of AGW plus 6 mL of inoculum yielded a total  $C_{\text{DIC}_{\text{blank}}} = 162 \mu\text{mol/L}$  and a  $\delta^{13}\text{C}_{\text{DIC}_{\text{blank}}} = -33.6\text{‰}$ . Some  $\text{CO}_2$  produced by the initial metabolic activity of bacteria in contact with urea may also contribute to the blank but it cannot be measured independently.

Our calculations indicate that the contaminating blank DIC induces a  $\sim 4.6\text{‰}$   $^{13}\text{C}$ -enrichment at the onset of ureolysis when the contribution of ureolysis-generated DIC is still low. Once ureolysis progress, the impact of the blank DIC is reduced. In the experiment with CA, after 30% AC, the  $\delta^{13}\text{C}_{\text{DIC}}$  offset induced by the blank becomes as low as  $0.5\text{‰}$  (Fig. B1 and Table B1). Blank-uncorrected  $\delta^{13}\text{C}_{\text{DIC}}$  values exhibit an initial decrease from  $-48.5$  to  $-58.3\text{‰}$  (up to %AC = 40%) followed by a final increase up to  $-48.9\text{‰}$ . Blank-corrected DIC values do not show this initial decrease, hence indicating that it was indeed linked to the initial presence of the blank DIC.

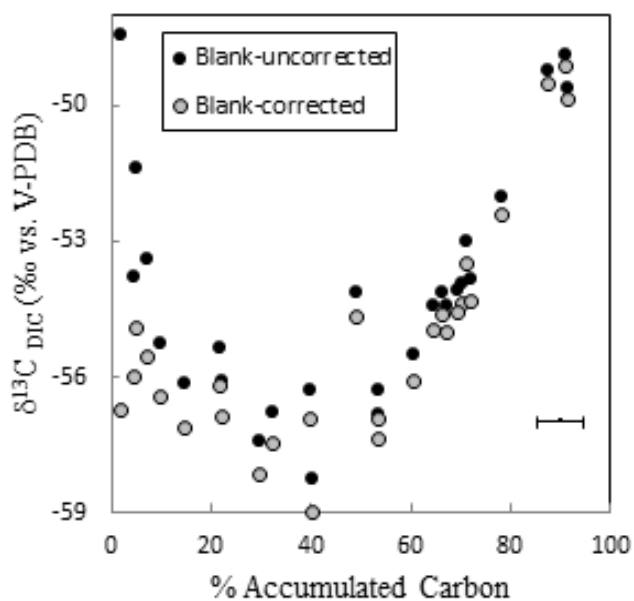


**Fig. B1.** Blank-uncorrected and blank-corrected  $\delta^{13}\text{C}$  values of the DIC as a function of ureolysis progress expressed using the accumulated product, with completion of the reaction at 100% (data obtained in the experiment with carbonic anhydrase). Black symbols refer to the experiment in the presence of CA (this study). Grey symbols refer to the experiment conducted without CA (Millo et al., 2012) and are plotted for comparison.

#### B4. Carbon systematics for the experiment with carbonic anhydrase

Carbonates whose  $\delta^{13}\text{C}$  values ( $\delta^{13}\text{C}_{\text{CaCO}_3}$ ) are presented in Fig. B2b and have precipitated from the blank-uncorrected DIC (Fig. B2a), which is the rationale for showing uncorrected data. In the experiment with CA, solid carbonate  $\delta^{13}\text{C}_{\text{CaCO}_3}$  values decreased from  $-55.6\text{‰}$  to  $-56.5\text{‰}$  (for  $\% \text{AC} = 40\%$ ) and finally increase up to  $\sim -54.1\text{‰}$  (Table B1).

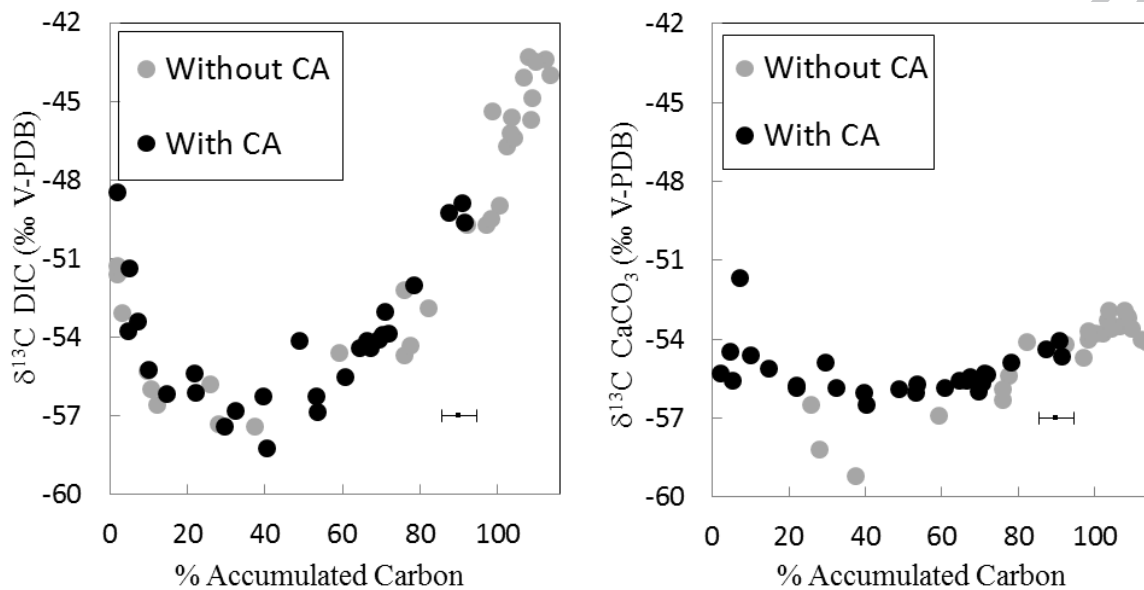


**Fig. B2.** (a)  $\delta^{13}\text{C}$  values of DIC (blank-uncorrected) and (b)  $\delta^{13}\text{C}$  values of precipitated  $\text{CaCO}_3$  plotted versus % Accumulated Carbon. Black symbols refer to the experiment in the presence of CA (this study). Grey symbols refer to the experiment conducted without CA (Millo et al., 2012) and are plotted for comparison. Vertical error bars in (a) and (b) are smaller than symbols.

**B5. Determination of the carbon isotopic signature of the accumulated product,  $\delta^{13}\text{C}_{\text{AC}}$** 

During ureolysis, carbon from urea is converted into DIC or solid carbonate, which taken together constitute the accumulated carbon produced by ureolysis (AC).  $\delta^{13}\text{C}_{\text{AC}}$  values were calculated by isotope and mass balance of precipitated  $\text{CaCO}_3$  and DIC corrected from blank contribution following Eq. (B1).  $\delta^{13}\text{C}_{\text{AC}}$  value is useful to determine the isotope fractionation factor associated with ureolysis and to assess the isotope balance at the end of the experiment.

$$\delta^{13}\text{C}_{\text{AC}} = \frac{n_{\text{corrected DIC}} \delta^{13}\text{C}_{\text{corrected DIC}} + n_{\text{CaCO}_3} \delta^{13}\text{C}_{\text{CaCO}_3}}{n_{\text{corrected DIC}} + n_{\text{CaCO}_3}} \quad (\text{B1})$$

The initial  $\delta^{13}\text{C}_{\text{AC}}$  value was  $\sim -56.0\text{‰}$  (Table B1 and Fig. B3).  $\delta^{13}\text{C}_{\text{AC}}$  value then progressively increased up to  $-52.3\text{‰}$  as ureolysis proceeded, thus remaining lower than the  $\delta^{13}\text{C}$  value of starting urea ( $\delta^{13}\text{C}_{0 \text{ urea}} = -48.9\text{‰}$ ; Millo et al. (2012)).

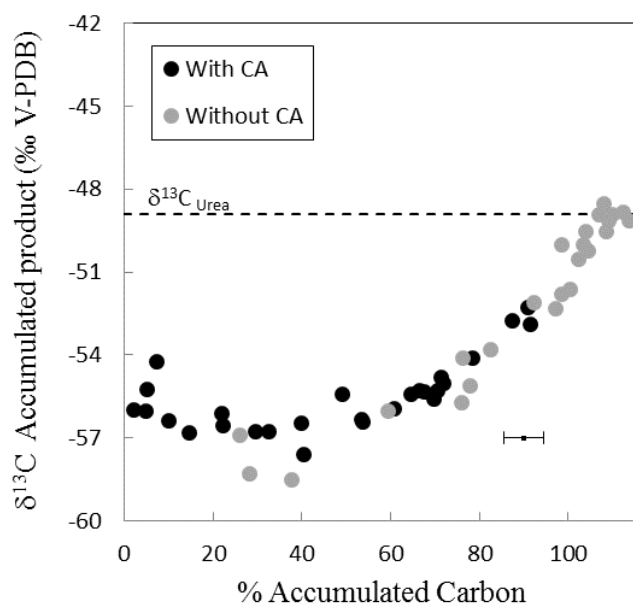


**Fig. B3.**  $\delta^{13}\text{C}$  values of Accumulated Carbon calculated by mass and isotope balance of DIC and precipitated  $\text{CaCO}_3$  (blank-corrected). Blank-corrected  $\delta^{13}\text{C}_{\text{AC}}$  strictly corresponds to the  $\delta^{13}\text{C}$  signature of inorganic carbon produced by ureolysis, without the contribution of the initial blank DIC. Black symbols refer to the experiment in the presence of CA (this study). Grey symbols refer to the experiment conducted without CA (Millo et al., 2012) and are plotted for comparison. Dashed line corresponds to the initial  $\delta^{13}\text{C}$  value of urea ( $\delta^{13}\text{C}_{0 \text{ urea}} = -48.9\text{‰}$ ). Vertical error bars are smaller than symbols.

As shown in Figs. B2 and B3, where data of both experiments with (this study) and without CA (Millo et al., 2012) are displayed for comparison, despite the fact that ureolysis did not reach completion in the experiment performed with CA (Fig.1), the patterns of  $\delta^{13}\text{C}_{\text{DIC}}$ ,  $\delta^{13}\text{C}_{\text{CaCO}_3}$ , and  $\delta^{13}\text{C}_{\text{AC}}$  values in both experiments are similar.

ACCEPTED MANUSCRIPT

### B.6. Determination of the ureolysis kinetic fractionation factor for C isotopes

The chemical system under study is closed with respect to atmosphere (i.e., no headspace in the Exetainer<sup>®</sup> vials capped with rubber septa). Urea is thus the only source of inorganic carbon during the whole course of the experiment (except for the blank DIC which is proportionally important in the first minutes only). As previously defined, during ureolysis, carbon from urea is converted into DIC or solid carbonate, which taken together constitute the accumulated carbon produced by ureolysis (AC). Note that AC was referred to as accumulated product (AP) by Millo et al. (2012). At the end of the experiment without CA,  $\delta^{13}\text{C}_{\text{AC}}$  (B1) value reached  $-48.9\text{‰}$ , which equals the initial  $\delta^{13}\text{C}$  value of urea and confirms full conversion of carbon from urea into both DIC and  $\text{CaCO}_3$  (i.e.,  $\% \text{AC} = 100$ ; Table B12 and Fig. B3). In the experiment with CA, considering that ureolysis did not proceed to completion (Fig.1) ( $\% \text{AC} = 91.4\%$ ), a lower final  $\delta^{13}\text{C}_{\text{AC}}$  value of  $-52.3\text{‰}$  is coherently observed (Table B1 and Fig. B3).

Millo et al. (2012) modeled the evolution of the  $\delta^{13}\text{C}_{\text{AC}}$  values as a function of ureolysis yield using a Rayleigh distillation equation (e.g., Mariotti et al., 1981):

$$\delta^{13}\text{C}_{\text{AC Rayleigh}} = (\delta^{13}\text{C}_{0\text{urea}} + 10^3) \times \frac{1 - (1 - f)^{\alpha_{\text{AC-urea}}}}{f} - 10^3 \quad (\text{B2})$$

where  $\delta^{13}\text{C}_{0\text{urea}}$  value is the initial carbon isotopic composition of urea,  $f$  is the fraction of DIN produced ( $f = [\text{DIN}] / 2[\text{urea}]_0$ ), and  $\alpha_{\text{AC-urea}}$  is the kinetic isotope fractionation factor associated with ureolysis. From this modeling, a  $1000\ln\alpha_{\text{AC-urea}}$  value of  $-12.5\text{‰}$  was obtained (Millo et al., 2012).

In the presence of CA and similarly to what was observed for the experiment without CA (Millo et al., 2012), the evolution pattern of  $\delta^{13}\text{C}_{\text{AC}}$  values was also best modeled assuming that  $1000\ln\alpha_{\text{AC-urea}} = -12.5\text{‰}$ . Such a negative kinetic fractionation factor value denotes preferential incorporation of  $^{12}\text{C}$  into the ureolysis product, in line with what is generally reported for bacterially-catalyzed reactions, (e.g., Coleman et al., 1981; Heraty et al., 1999; Miller et al., 2001, 2004; Brungard et al., 2003).

**B7. Determination of  $1000\ln\alpha_{\text{CaCO}_3\text{-HCO}_3^-}$  for carbon isotopes**

If precipitation occurred at carbon isotope equilibrium between DIC and solid carbonate, then  $1000\ln\alpha_{\text{CaCO}_3\text{-HCO}_3^-}$  would be equal to 0.96‰, as established for calcite at 30°C (Zhang et al., 1995; Romanek et al., 1992). Isotopic fractionation between  $\text{CaCO}_3$  and DIC is expressed as the isotopic difference between  $\text{CaCO}_3$  and  $\text{HCO}_3^-$ , which is the most abundant DIC species in our experiment at the encountered pH.  $\delta^{13}\text{C}_{\text{HCO}_3^-}$  values were derived from the measured  $\delta^{13}\text{C}_{\text{DIC}}$  value by considering the carbon isotope fractionation factors given for the equilibrium reactions between the DIC species, as proposed by Zhang et al. (1995).  $\delta^{13}\text{C}_{\text{HCO}_3^-}$  values for each sample were calculated based on the relative abundances of  $\text{H}_2\text{CO}_3$ ,  $\text{HCO}_3^-$  and  $\text{CO}_3^{2-}$ . Coherently, the pH-dependent speciation of DIC (calculated with JCHESS<sup>®</sup>) indicated a dominance of  $\text{HCO}_3^-$  (56.7 to 91.6% of the total DIC) over  $\text{CO}_3^{2-}$  (7.9 to 43.3% of the total DIC), whereas  $\text{CO}_{2(\text{aq})}$  was negligible ( $\leq 0.5\%$ ) (Table B1).

(i) The trend of the calculated  $\delta^{13}\text{C}_{\text{HCO}_3^-}$  values plotted as a function of  $C_{\text{CaCO}_3}$  can be approximated by a  $\delta^{13}\text{C}_{\text{HCO}_3^- \text{BF}}$  value derived from a best-fit curve equation (Fig. B4a), as follows:

$$\delta^{13}\text{C}_{\text{HCO}_3^- \text{BF}} = a \cdot (C_{\text{CaCO}_3})^2 + b \cdot (C_{\text{CaCO}_3}) + d \quad (\text{B3})$$

where BF stands for “best-fit”,  $a = 0.06$ ,  $b = -0.9$  and  $d = -54$ .

(ii) The  $\delta^{13}\text{C}$  value of  $\text{CaCO}_3$  instantaneously precipitated during ureolysis ( $\delta^{13}\text{C}_{\text{inst. CaCO}_3}$ ) is expressed by the following equation:

$$\delta^{13}\text{C}_{\text{inst. CaCO}_3} = \delta^{13}\text{C}_{\text{HCO}_3^- \text{BF}} + 1000\ln\alpha_{\text{CaCO}_3\text{-HCO}_3^-} \quad (\text{B4})$$

where  $1000\ln\alpha_{\text{CaCO}_3\text{-HCO}_3^-}$  is the carbon isotope fractionation factor between  $\text{CaCO}_3$  and  $\text{HCO}_3^-$  during carbonate precipitation.

(iii) Considering that no reequilibration between solid  $\text{CaCO}_3$  and DIC occurred, the  $\delta^{13}\text{C}_{\text{acc. CaCO}_3}$  value, being the cumulative sum of  $\delta^{13}\text{C}_{\text{inst. CaCO}_3}$  values weighted by molar  $\text{CaCO}_3$  accumulation, is then computed as the integral of the instantaneous  $\text{CaCO}_3$  function ( $\delta^{13}\text{C}_{\text{inst. CaCO}_3}$ ) for the whole precipitation interval that is from the beginning through the end of  $\text{CaCO}_3$  precipitation:

$$\delta^{13}\text{C}_{\text{acc. CaCO}_3} = \frac{1}{n - n_0} \int_{n_0}^n \delta^{13}\text{C}_{\text{inst. CaCO}_3} \, dn \quad (\text{B5})$$

where  $n_0 = 0$  and  $n$  is the  $n_{\text{CaCO}_3}$  value measured at the end of the experiment.

Combining Eqs. B3, B4 and B5 yields:

$$\delta^{13}\text{C}_{\text{acc. CaCO}_3} = \frac{a}{3} n^2 + \frac{b}{2} n + c + 1000\ln\alpha_{\text{CaCO}_3\text{-HCO}_3^-} \quad (\text{B6})$$

The resulting  $\delta^{13}\text{C}_{\text{acc.CaCO}_3}$  value curve calculated assuming precipitation at carbon isotope equilibrium for calcite yielded an imperfect match with measured  $\delta^{13}\text{C}_{\text{CaCO}_3}$  values, especially at the beginning of precipitation (Fig. B4).

### $\delta^{13}\text{C}$ error calculation model

Errors for  $\delta^{13}\text{C}_{\text{HCO}_3^- \text{BF}}$ , and hence  $\delta^{13}\text{C}_{\text{inst.CaCO}_3}$ , were estimated by comparing the  $\delta^{13}\text{C}_{\text{HCO}_3^- \text{BF}}$  best-fit curve to the experimental  $\delta^{13}\text{C}_{\text{HCO}_3^-}$  values with a non-linear regression. The uncertainty was found to be  $\pm 1.6\%$  ( $1\sigma$ ). Error for  $\delta^{13}\text{C}_{\text{acc.CaCO}_3}$  (which is a weighted average of  $\delta^{13}\text{C}_{\text{inst.CaCO}_3}$ ) was calculated from errors on  $\delta^{13}\text{C}_{\text{inst.CaCO}_3}$  ( $\pm 1.6$  ( $1\sigma$ )) and on  $n_{\text{CaCO}_3}$  (deduced from error on  $\text{Ca}^{2+}$  concentrations from ICP-AES measurements which was of  $\pm 0.001$  ( $1\sigma$ )). The main source of uncertainty being that on  $\delta^{13}\text{C}_{\text{inst.CaCO}_3}$ , the error on  $\delta^{13}\text{C}_{\text{acc.CaCO}_3}$  values can be simplified as:

$$\sigma_{\delta^{13}\text{C}_{\text{acc.CaCO}_3}} \approx \frac{1.6}{\sqrt{n}} \quad (\text{B7})$$

with  $n$  the number of samples in the experiment from which we build the best-fit.

Considering  $n$  varying from 1 to 27, the error on  $\delta^{13}\text{C}_{\text{acc.CaCO}_3}$  values ranged from  $\pm 1.2\%$  to  $\pm 0.3\%$ .

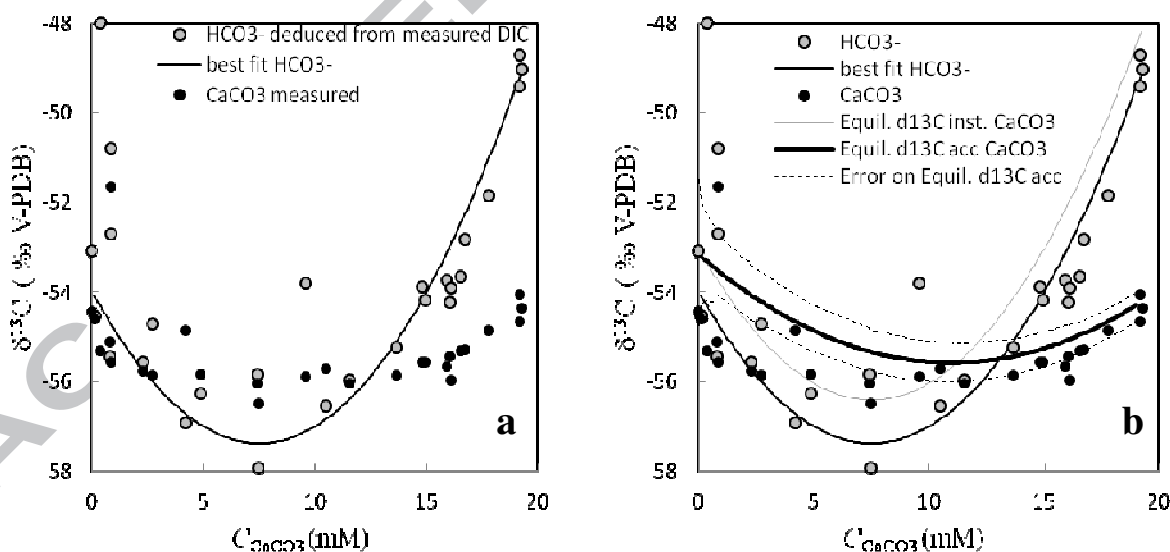


**Fig. B4.** Carbon isotope data obtained in the experiment with carbonic anhydrase and plotted against  $C_{\text{CaCO}_3}$ . Horizontal error bars are smaller than symbols. (a)  $\delta^{13}\text{C}$  values of precipitated  $\text{CaCO}_3$  (measured) and  $\text{HCO}_3^-$  (calculated) and its best-fit curve (thin black line);  $\delta^{13}\text{C}_{\text{HCO}_3^- \text{BF}}$  displays an error of  $\pm 1.6\%$ ; (b) Modeling of the evolution of the instantaneous  $\delta^{13}\text{C}$  values of precipitated  $\text{CaCO}_3$  calculated from with  $\delta^{13}\text{C}_{\text{HCO}_3^- \text{BF}}$  values assuming

carbonate precipitation at isotopic equilibrium with a constant carbon isotope fractionation factor  $1000\ln\alpha_{\text{CaCO}_3\text{-HCO}_3^-}$  of 0.96‰ (Equil.  $\delta^{13}\text{C}_{\text{inst.CaCO}_3}$ ; light gray curve). Also shown is the modeling of the  $\delta^{13}\text{C}$  values of  $\text{CaCO}_3$  accumulated over the course of the batch experiment (Equil.  $\delta^{13}\text{C}_{\text{acc.CaCO}_3}$ ; bold black curve); the dashed line corresponds to the upper and lower limits of error propagation. Data points are the same as in (a).

Assuming that the  $1000\ln\alpha_{\text{CaCO}_3\text{-HCO}_3^-}$  value may deviate from equilibrium at the beginning of precipitation, we thus recalculated the evolution of  $\delta^{13}\text{C}_{\text{acc.CaCO}_3}$  values using variable  $1000\ln\alpha_{\text{CaCO}_3\text{-HCO}_3^-}$ , until we found a good match between the obtained  $\delta^{13}\text{C}_{\text{acc.CaCO}_3}$  curve and the trend defined by measured  $\delta^{13}\text{C}_{\text{CaCO}_3}$  values. The best-fit between newly calculated  $\delta^{13}\text{C}_{\text{acc.CaCO}_3}$  values and measured  $\delta^{13}\text{C}_{\text{CaCO}_3}$  ones shown in Fig B5a was obtained assuming an initial out of equilibrium fractionation factor of  $\sim -2\text{‰}$ . Values for  $1000\ln\alpha_{\text{CaCO}_3\text{-HCO}_3^-}$  then converged toward the carbon isotope equilibrium fractionation value of 0.96‰ as precipitation proceeded to completion (Fig. B5b). This range of values coincides with that found in the experiment without CA (Millo et al., 2012) where an offset from carbon isotope equilibrium of  $-1.9\text{‰}$  was also identified at the beginning of the experiment. This offset from equilibrium for carbon isotopes is probably linked to a kinetic isotope fractionation associated with the high precipitation rate at the beginning of the experiment, as suggested by Millo et al. (2012). Alternatively and not mutually exclusively, it could be due to the probable predominance of vaterite compared to calcite and aragonite at the beginning of precipitation.

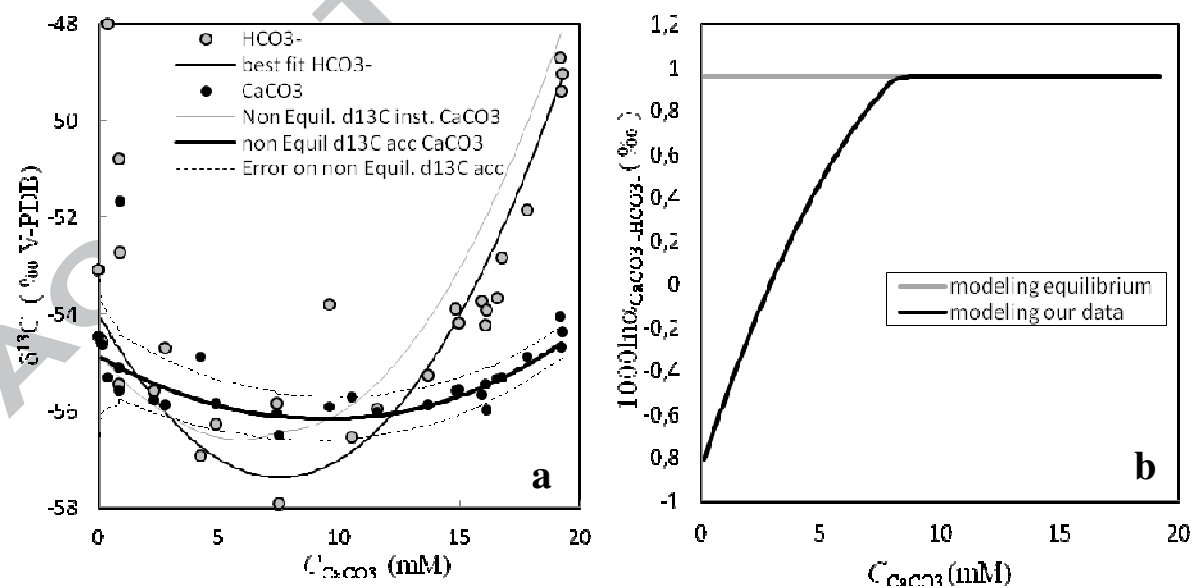


**Fig. B5.** Carbon isotope data obtained in the experiment with carbonic anhydrase and plotted against  $n_{\text{CaCO}_3}$ . Horizontal error bars are smaller than symbols. (a) Modeling of the evolution of  $\delta^{13}\text{C}_{\text{inst.CaCO}_3}$  and  $\delta^{13}\text{C}_{\text{acc.CaCO}_3}$

performed assuming that precipitation initiates out of isotopic equilibrium with  $\text{HCO}_3^-$ . Symbols and data points are the same as in Fig. B4. (b) The model prescribed a variable carbon isotope fractionation factor between  $\text{CaCO}_3$  and  $\text{HCO}_3^-$  whose evolution is shown by the dashed black line. Initial fractionation was of  $\sim -2\text{‰}$  and increased progressively to a value of  $+0.96\text{‰}$  where it remained constant for the rest of the precipitation sequence.

Overall, these calculations demonstrated that precipitation occurred mainly at carbon isotope equilibrium between solid carbonates and DIC and without isotopic reequilibration between  $\text{CaCO}_3$  and DIC in the experiment with CA, as it was also the case in the one without CA (Millo et al. 2012). The carbon isotope systematics of both ureolysis and carbonate precipitation was thus similar in the presence and in the absence of CA. This indicates that CA activity exerted no influence on the carbon isotopes systematics of bacterially-induced ureolysis and associated carbonate precipitation, similarly to what was observed during abiotic carbonate precipitation experiments performed by Uchikawa and Zeebe (2012).

Table B1. Carbon isotope data obtained during the batch experiment of ureolysis and  $\text{CaCO}_3$  precipitation induced by *S. pasteurii*. with carbonic anhydrase. For carbon isotope values of the experiment performed without CA, the reader is referred to Millo et al. (2012).

Reaction time (min)	%AC ( $\sigma = \pm 5\%$ )	Blank–uncorrected $\delta^{13}\text{C}_{\text{DIC}}$ (‰ vs. V–PDB) ( $\sigma = \pm 0.1\text{‰}$ )	Blank–corrected $\delta^{13}\text{C}_{\text{DIC}}$ (‰ vs. V–PDB) ( $\sigma = \pm 0.1\text{‰}$ )	Blank–uncorrected $\delta^{13}\text{C}_{\text{HCO}_3^-}$ (‰ vs. V–PDB) ( $\sigma = \pm 0.1\text{‰}$ )	$\delta^{13}\text{C}_{\text{CaCO}_3}$ (‰ vs. V–PDB) ( $\sigma = \pm 0.08\text{‰}$ )	Blank–corrected $\delta^{13}\text{C}_{\text{AC}}$ (‰ vs. V–PDB) ( $\sigma = \pm 0.1\text{‰}$ )
20	2.1	-48.5	-56.7	-48.0	-55.3	-56.0
27	5.1	-51.4	-54.9	-50.8	-55.6	-55.2
40	7.3	-53.4	-55.6	-52.7	-51.7	-54.2
50	4.7	-53.8	-56.0	-53.1	-54.5	-56.0
69	9.9	-55.3	-56.4	-54.5	-54.6	-56.4
83	14.7	-56.2	-57.1	-55.4	-55.1	-56.8
94	22.0	-55.4	-56.2	-54.7	-55.9	-56.1
116	22.1	-56.1	-56.9	-55.6	-55.8	-56.5
127	29.6	-57.4	-58.1	-56.9	-54.9	-56.7
142	32.5	-56.8	-57.5	-56.3	-55.9	-56.7
156	39.7	-56.3	-56.9	-55.8	-56.0	-56.4
186	49.0	-54.1	-54.7	-53.8	-55.9	-55.4
219	40.4	-58.3	-59.0	-57.9	-56.5	-57.6
247	53.6	-56.8	-57.4	-56.5	-55.7	-56.4
275	53.4	-56.3	-56.9	-56.0	-56.0	-56.3
303	60.8	-55.5	-56.1	-55.2	-55.9	-55.9
334	66.4	-54.1	-54.6	-53.9	-55.6	-55.3
369	64.6	-54.4	-55.0	-54.2	-55.6	-55.4
394	70.5	-53.9	-54.4	-53.7	-55.7	-55.3
404	67.4	-54.4	-55.0	-54.2	-55.4	-55.3
405	71.9	-53.8	-54.3	-53.7	-55.3	-55.0
424	69.6	-54.1	-54.6	-53.9	-56.0	-55.6
454	71.2	-53.0	-53.5	-52.8	-55.3	-54.8

481	78.4	-52.0	-52.4	-51.8	-54.9	-54.1
24h	90.8	-48.9	-49.1	-48.7	-54.1	-52.3
24h	87.4	-49.2	-49.5	-49.0	-54.4	-52.7
24h	91.4	-49.6	-49.9	-49.4	-54.7	-52.9

(a)  $\delta^{13}\text{C}_{\text{HCO}_3^-}$  values were calculated as indicated in Appendix B7

(b)  $\delta^{13}\text{C}_{\text{AC}}$  denotes  $\delta^{13}\text{C}$  value of the accumulated Blank-corrected DIC+CaCO<sub>3</sub> (Eq.B1).

## Appendix B references

Assayag N., Rivé K., Ader M., Jézéquel D. and Agrinier P. (2006) Improved method for isotopic and quantitative analysis of dissolved inorganic carbon in natural water samples. *Rapid Commun. Mass Spectrom.* **20**, 2243–2251.

Brungard K. L., Munakata–Marr J., Johnson C. A. and Mandernack K. W. (2003) Stable carbon isotope fractionation of trans–1,2–dichloroethylene during co–metabolic degradation by methanotrophic bacteria. *Chem. Geol.* **195**, 59–67.

Coleman D. D., Risatti J. B. and Schoell M. (1981) Fractionation of carbon and hydrogen isotopes by methane–oxidizing bacteria. *Geochim. Cosmochim. Acta* **45**, 1033–1037.

Heraty L. J., Fuller M. E., Huang L., Abrajano, Jr., T. and Sturchio N. C. (1999) Isotopic fractionation of carbon and chlorine by microbial degradation of dichloromethane. *Org. Geochem.* **30**, 793–799.

Horita J. and Kendall C. (2004) Stable isotope analysis of water and aqueous solutions by conventional dual-inlet mass spectrometry. In *Handbook of Stable Isotope Analytical Techniques* (eds P. A. d. Groot) Elsevier, Amsterdam, pp. 1–37

Mariotti A., Germon J. C., Hubert P., Kaiser P., Letolle R., Tardieux A. and Tardieux P. (1981) Experimental determination of nitrogen kinetic isotope fractionation: Some principles; illustration for the denitrification and nitrification processes. *Plant Soil* **62**, 413–430.

Miller L. G., Kalin R. M., McCauley S. E., Hamilton J. T. G., Harper D. B., Millet D. B., Oremland R. S. and Goldstein A. H. (2001) Large carbon isotope fractionation associated with oxidation of methyl halides by methylotrophic bacteria. *P. Natl. Acad. Sci. USA* **98**, 5833–5837.

- Miller L. G., Warner K. L., Baesman S. M., Oremland R. S., McDonald I. R., Radajewski S. and Murrell J. C. (2004) Degradation of methyl bromide and methyl chloride in soil microcosms: Use of stable C isotope fractionation and stable isotope probing to identify reactions and the responsible microorganisms. *Geochim. Cosmochim. Acta* **68**, 3271–3283.
- Millo C., Dupraz S., Ader M., Guyot F., Thaler C., Foy E. and Ménez B. (2012). Carbon isotope fractionation during calcium carbonate precipitation induced by ureolytic bacteria. *Geochim. Cosmochim. Acta* **98**, 107–124.
- Romanek C. S., Grossman E. L. and Morse J. W. (1992) Carbon isotope fractionation in synthetic aragonite and calcite: Effects of temperature and precipitation rate. *Geochim. Cosmochim. Acta* **56**, 419–430.
- Uchikawa J. and Zeebe R. E. (2012) The effect of carbonic anhydrase on the kinetics and equilibrium of the oxygen isotope exchange in the CO<sub>2</sub>–H<sub>2</sub>O system: Implications for  $\delta^{18}\text{O}$  vital effects in biogenic carbonates. *Geochim. Cosmochim. Acta*, **95**, 15–34.
- Zhang J., Quay P. D. and Wilbur D. O. (1995) Carbon isotope fractionation during gas–water exchange and dissolution of CO<sub>2</sub>. *Geochim. Cosmochim. Acta* **59**, 107–114.

**Appendix C.****C1.  $\delta^{18}\text{O}_{\text{CaCO}_3}$  and  $1000\ln\alpha_{\text{CaCO}_3\text{-H}_2\text{O}}$  equilibrium values calculations**

We have calculated possible equilibrium  $\delta^{18}\text{O}_{\text{CaCO}_3}$  values for calcite precipitated in our experiments based on three different sets of equations from the literature (Kim and O'Neil, 1997; Coplen, 2007; Chacko and Deines, 2008) and also use Zeebe (2007) Dietzel et al., (2009) and Gabitov et al., (2012) to discriminate different fractionating processes. When it is not specified, we made calculation using  $T = 30^\circ\text{C}$  and  $\delta^{18}\text{O}_{\text{H}_2\text{O}} = -6.8 \pm 0.1 \text{‰}$ . In all calculations, the temperature  $T$  is in Kelvin. Equilibrium  $\delta^{18}\text{O}_{\text{CaCO}_3}$  values for our experiment are calculated with the  $\delta^{18}\text{O}_{\text{H}_2\text{O}}$  in the experiment with CA in order to compare them with the measured  $\delta^{18}\text{O}_{\text{CaCO}_3}$  and are given with respect to V-SMOW.

**According to Chacko and Deines (2008):**

The equation has been established for temperature ranging from 0 to  $900^\circ\text{C}$ .

Equation used:  $1000\ln\alpha_{\text{CaCO}_3\text{-H}_2\text{O}} = 1000\ln\beta_{\text{CaCO}_3} - 1000\ln\beta_{\text{H}_2\text{O}}$

$$1000\ln\beta = C_0 + C_1 \cdot x - C_2 \cdot 10^{-1} \cdot x^2 + C_3 \cdot 10^{-2} \cdot x^3 - C_4 \cdot 10^{-3} \cdot x^4 + C_5 \cdot 10^{-5} \cdot x^5 - C_6 \cdot 10^{-6} \cdot x^6$$

with  $x = 10^6/T$

Constants  $C_0, C_1, C_2, C_3, C_4, C_5, C_6$  are for calcite and water, respectively:

Calcite: 0; 11.75; 4.6655; 3.1252; 1.8869; 7.4768; 1.3404

Water: 12.815; 6.237; 1.254; 0.2419; 0; 0; 0

$$1000\ln\alpha_{\text{CaCO}_3\text{-H}_2\text{O}} = 26.65$$

$$\delta^{18}\text{O}_{\text{CaCO}_3\text{equilibrium}} = 20.07\text{‰}$$

**According to Coplen (2007):**

The equation gives satisfactory results for temperature ranging from 13 to  $40^\circ\text{C}$ .

Equation used:  $1000\ln\alpha_{\text{CaCO}_3\text{-H}_2\text{O}} = 17400/T - 28.6$

$$1000\ln\alpha_{\text{CaCO}_3\text{-H}_2\text{O}} = 28.80$$

$$\delta^{18}\text{O}_{\text{CaCO}_3\text{equilibrium}} = 22.26\text{‰}$$

**According to Kim and O'Neil (1997):**

The equation has been established for a temperature range from 10 to  $40^\circ\text{C}$ .

Equation used:  $1000\ln\alpha_{\text{CaCO}_3\text{-H}_2\text{O}} = 18030/T - 32.42$

Thaler et al.,

$$1000\ln\alpha_{\text{CaCO}_3\text{-H}_2\text{O}} = 27.06$$

$$\delta^{18}\text{O}_{\text{CaCO}_3\text{equilibrium}} = 20.48\text{‰}$$

**According to Zeebe (2007):**

We used the Excel routine given in the auxiliary material of the manuscript and working from 0 to 50°C. Input data are temperature, pH and salinity. We obtained salinity values for each samples thanks to JCHESS<sup>®</sup> modeling. pH are displayed in Table 1.

$$27.9 < 1000\ln\alpha_{\text{CaCO}_3\text{-H}_2\text{O}} < 29.3$$

$$21.38\text{‰} < \delta^{18}\text{O}_{\text{CaCO}_3\text{equilibrium}} < 22.85\text{‰}$$

For the final pH 8.7, we obtain  $1000\ln\alpha_{\text{CaCO}_3\text{-H}_2\text{O}} = 28.8$

**According to Gabitov et al. (2012):**

The equation has been established for temperature ranging from 15 to 25°C. We extrapolated it at 30°C. It gives  $1000\ln\alpha_{\text{CaCO}_3\text{-H}_2\text{O}}$  for calcite grown at 0.2 nm/s that are not supposed to be at equilibrium because of their precipitation rate.

$$\text{Equation used: } 1000\ln\alpha_{\text{CaCO}_3\text{-H}_2\text{O}} = 17746/T - 30.238$$

$$1000\ln\alpha_{\text{CaCO}_3\text{-H}_2\text{O}} = 28.30$$

$$\delta^{18}\text{O}_{\text{CaCO}_3\text{equilibrium}} = 21.75\text{‰}$$

**According to Dietzel et al. (2009):**

The equation has been established at 25°C and 40°C; we have chosen the equation at 25°C.

Equation used:  $1000\ln\alpha_{\text{CaCO}_3\text{-H}_2\text{O}} = -1.094 \log R + 30.87$ , with  $R$  displayed in Table 1.

$$4.41 < \log R < 5.57$$

$$24.9 < 1000\ln\alpha_{\text{CaCO}_3\text{-H}_2\text{O}} < 26.0$$

$$18.14\text{‰} < \delta^{18}\text{O}_{\text{CaCO}_3\text{equilibrium}} < 19.44\text{‰}$$

## C2. Calculation of the relative proportions of hydration and hydroxylation

The proportion of hydrated and hydroxylated  $\text{CO}_2$  in aqueous solution depends on pH (that controls DIC speciation), but also on temperature and solution salinity, both influencing the reaction rates. All the equations here used to calculate the proportion of hydration versus hydroxylation are described in Zeebe and Wolf-Gladrow (2001).  $k_1$  and  $k_2$  reaction constants as a function of salinity and temperature can be found in Millero et al. (2002);  $k_w$  (water dissociation constant) can be found in Millero (1995). For our experimental conditions (temperature of  $30^\circ\text{C}$  and salinity of  $6.4\text{ kg/L}$ ) we obtain the distribution shown in Fig. C1.

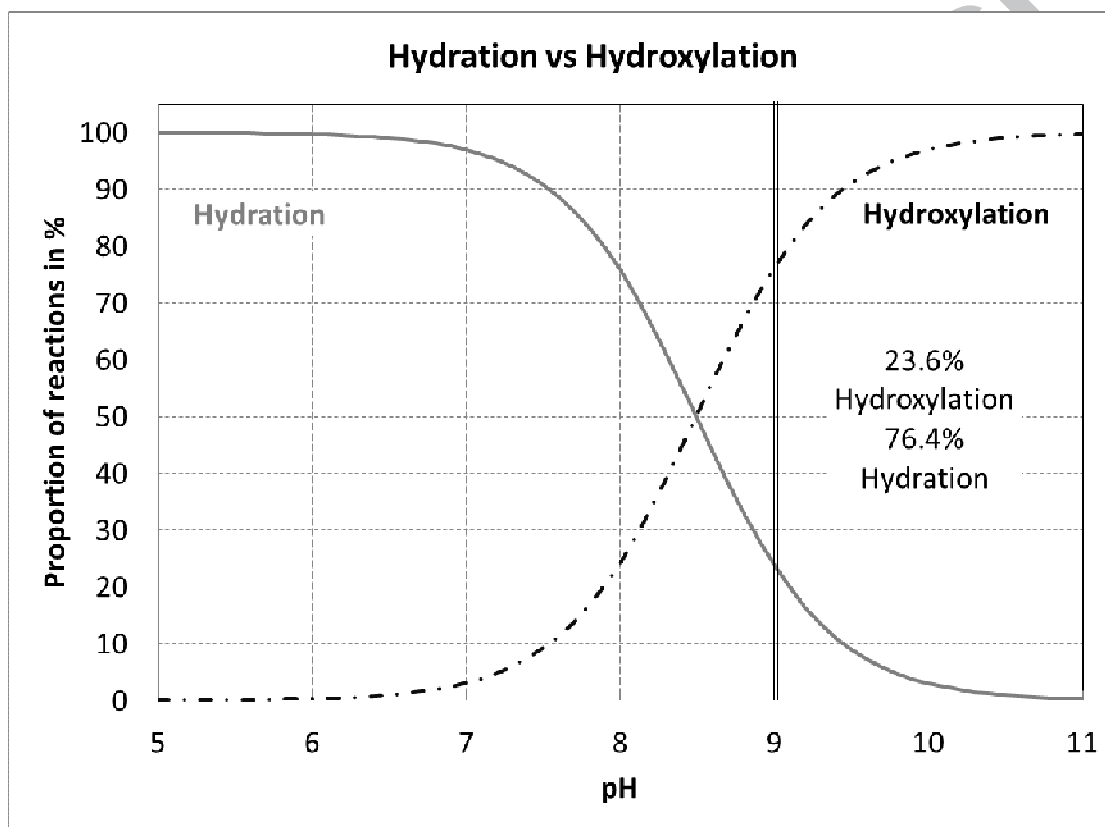


**Fig. C1.** Proportion of hydrated and hydroxylated  $\text{CO}_2$  at  $30^\circ\text{C}$  and for a salinity of  $6.4\text{ kg/L}$ . At pH 9, 23.6% of  $\text{CO}_2$  is hydroxylated and 76.4% is hydrated. We evaluated these proportions at pH 9 because it corresponds to the pH at the beginning of the precipitation when the most important isotopic disequilibrium is observed for oxygen between solid carbonates and water. Note that at the end of the reaction pH is lower and the percentage of hydroxylation should be lower, hence decreasing the overall isotope effect.

## Appendix C references

Chacko T. and Deines P. (2008) Theoretical calculation of oxygen isotope fractionation factors in carbonate systems. *Geochim. Cosmochim. Acta* **72**, 3642–3660.

- Coplen T. B. (2007) Calibration of the calcite–water oxygen-isotope geothermometer at Devils Hole, Nevada, a natural laboratory. *Geochim. Cosmochim. Acta* **71**, 3948–3957.
- Dietzel M., Tang J., Leis A. and Koehler S. J. (2009) Oxygen isotopic fractionation during inorganic calcite precipitation – Effects of temperature, precipitation rate and pH. *Chem. Geol.* **268**, 107–115.
- Gabitov R. I., Watson E. B. and Sadekov A. (2012) Oxygen isotope fractionation between calcite and fluid as a function of growth rate and temperature: An in situ study. *Chem. Geol.* **306**, 92–102.
- Kim S. T. and O'Neil J. R. (1997) Equilibrium and nonequilibrium oxygen isotope effects in synthetic carbonates. *Geochim. Cosmochim. Acta* **61**, 3461–3475.
- Millero F. J. (1995) Thermodynamics of the carbon dioxide system in the oceans. *Geochim. Cosmochim. Acta* **59**, 661–677.
- Zeebe R. E. (2007) An expression for the overall oxygen isotope fractionation between the sum of dissolved inorganic carbon and water. *Geochem. Geophys. Geosyst.* **8**, Q09002, doi:10.1029/2007GC001663.
- Zeebe R. E. and Wolf-Gladrow D. (2001) *CO<sub>2</sub> in seawater: Equilibrium, kinetics, isotopes*. Elsevier oceanography series **65**, the Netherlands, pp 346.

**FIGURE CAPTIONS**

Fig. 1. Comparative evolution of the experiments performed with and without carbonic anhydrase (CA): (a) Time course evolution of ureolysis yield expressed in terms of Accumulated Dissolved Inorganic Nitrogen (DIN) in mM (see section 3.1); (b) Evolution as a function of time of % Accumulated Carbon (see section 3.1) representing the quantity of carbon from urea converted during ureolysis. Black symbols refer to the experiment with CA conducted specifically for this study. Grey symbols refer to the experiment conducted in the absence of CA by Millo et al. (2012). Horizontal error bars in (a) are smaller than symbols, the horizontal error bar presented in figure 1b is the same for figure 1a.

Fig. 2. Comparative evolution of the chemical parameters measured in the course of the experiments performed with and without carbonic anhydrase (CA): (a) pH versus % Accumulated Carbon (%AC); (b) DIC concentrations ( $C_{DIC}$ ) versus %AC; (c) Precipitation yield (relative to the initial  $Ca^{2+}$  content in solution) versus %AC; Black symbols refer to the experiment with CA conducted specifically for this study. Grey symbols refer to the experiment conducted in the absence of CA by Millo et al. (2012). Vertical error bars are smaller than symbols in (a) and (c).

Fig. 3. SEM images of the calcium carbonate precipitates obtained in the experiment with CA (conducted for this study) at different reaction times: (a) backscattered electron image after 180 minutes of experiment; carbonates consisted mostly of half spheres of 5 to 10  $\mu\text{m}$  in diameter (more rarely of larger ones of 30  $\mu\text{m}$  in diameter) and of prisms of 30 to 50  $\mu\text{m}$  edge length; (b) backscattered electron image after 300 minutes of experiment; carbonates were aggregated rounded prisms of 70  $\mu\text{m}$  in size. Bacterial pockmarks can be seen on the surface; (c) and (d) secondary electron images after 24 hours of experiment; carbonates were regular half-spheres whose size mostly ranged from 70 to 100  $\mu\text{m}$  in diameter;

Fig. 4. Time course evolution of the carbonate precipitation rate expressed as  $\log R$ . Solid carbonates are assumed to be 100% vaterite (diamonds) at the onset of precipitation, and 100% calcite (circles) afterwards. Data of the experiment without CA (Millo et al., 2012) were reported for comparison.

Fig. 5. Evolution of  $1000\ln\alpha_{\text{CaCO}_3\text{-water}}$  values of carbonates precipitated during bacterial ureolysis plotted as a function of the molar quantity of precipitated  $\text{CaCO}_3$  ( $C_{\text{CaCO}_3}$ ). Black symbols refer to experiment with CA; grey symbols refer to experiment without CA. Solid curves are best-fit functions of measured  $1000\ln\alpha_{\text{CaCO}_3\text{-water}}$  data points. Dashed curves represent the evolution of  $1000\ln\alpha_{\text{CaCO}_3\text{-water}}$  values when considering an instantaneously precipitated  $\text{CaCO}_3$  (Section 4.3, Eq.26). Horizontal lines represent equilibrium values of  $1000\ln\alpha_{\text{CaCO}_3\text{-water}}$  calculated for our experimental temperature, according to the authors indicated next to each line. An equilibrium range encompassing these values was established in accordance.

Fig. 6. Correlation between  $\delta^{13}\text{C}$  and  $\delta^{18}\text{O}$  values of  $\text{CaCO}_3$  precipitated in the experiment without CA ( $\delta^{18}\text{C}_{\text{CaCO}_3}$  are from Millo et al., 2012). The correlation could either be explained by a Rayleigh distillation involving both C and O isotopes, or a Rayleigh distillation involving only the C isotopes, combined with an oxygen isotope equilibration between DIC and  $\text{H}_2\text{O}$ .  $\delta^{13}\text{C}$  data are given in the appendix. Error bars are smaller than symbols.

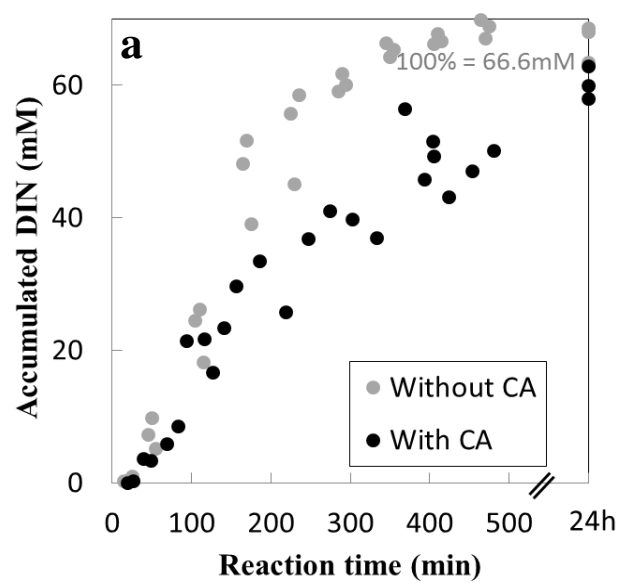
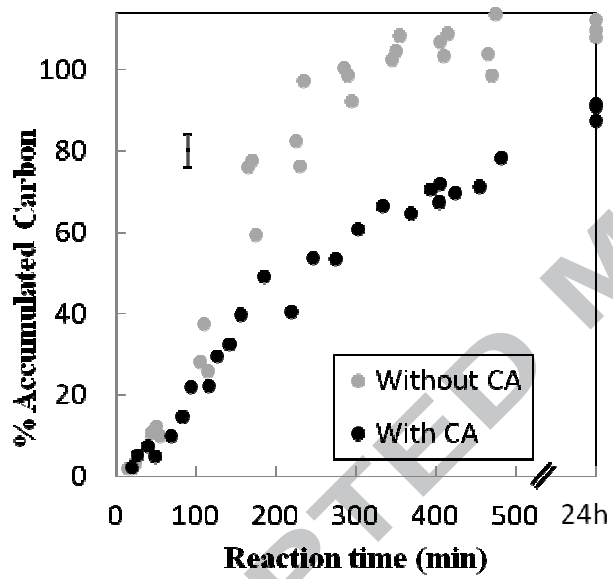
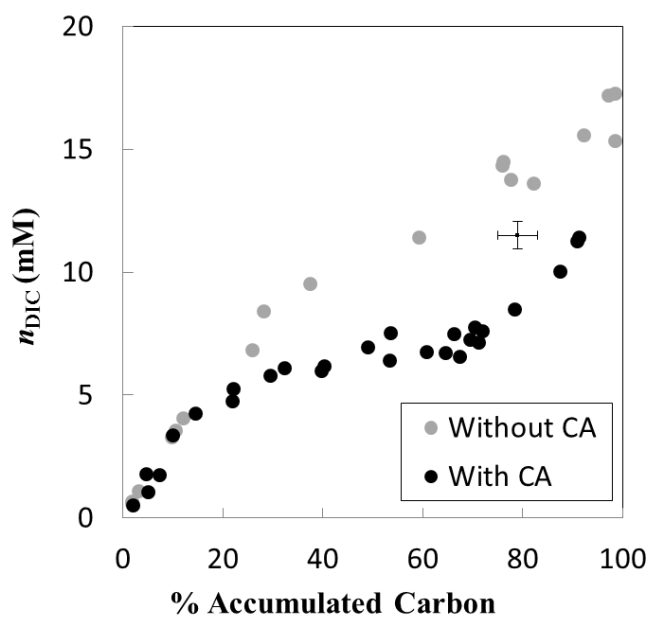
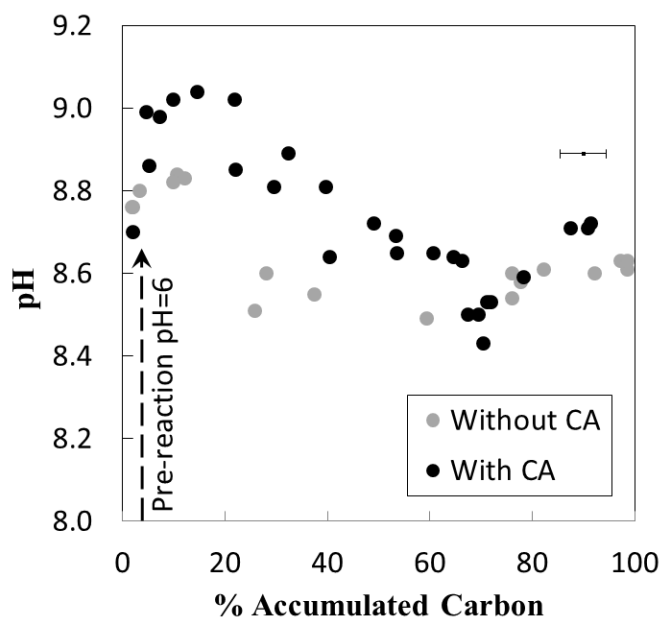
**b**

Fig.1(a and b)



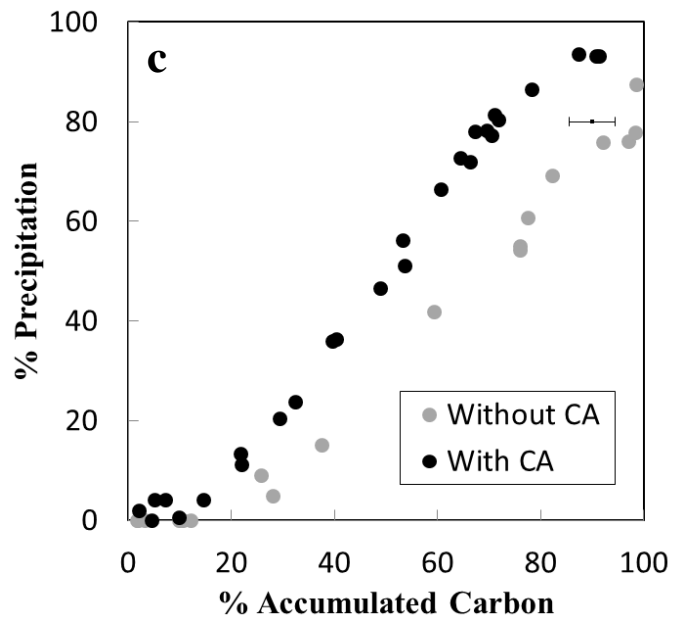
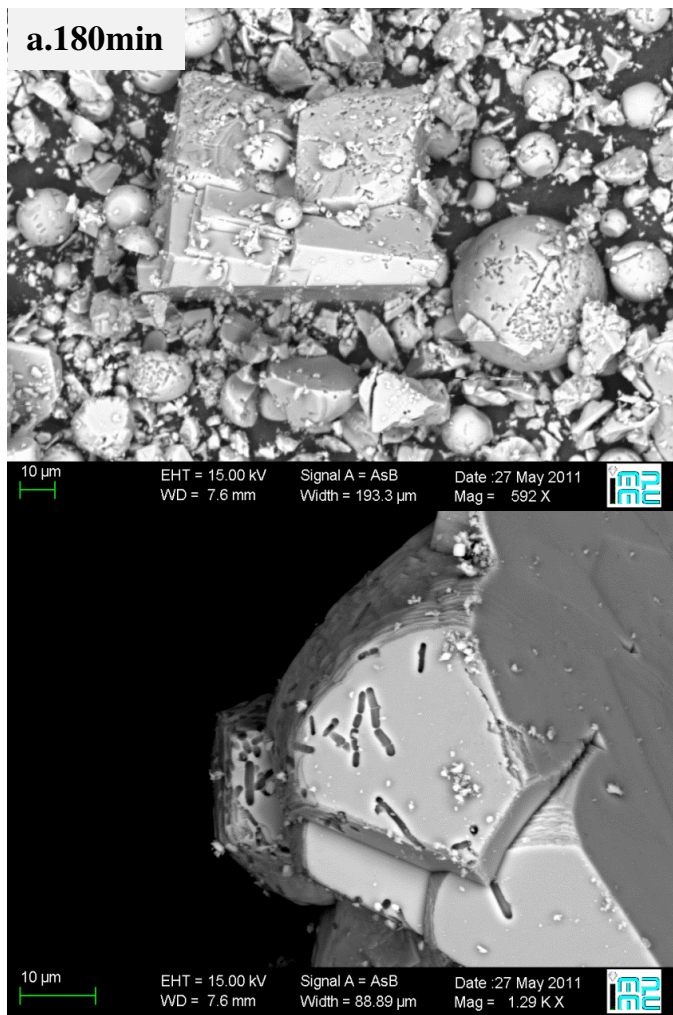


Fig. 2.(a, b and c)



300min

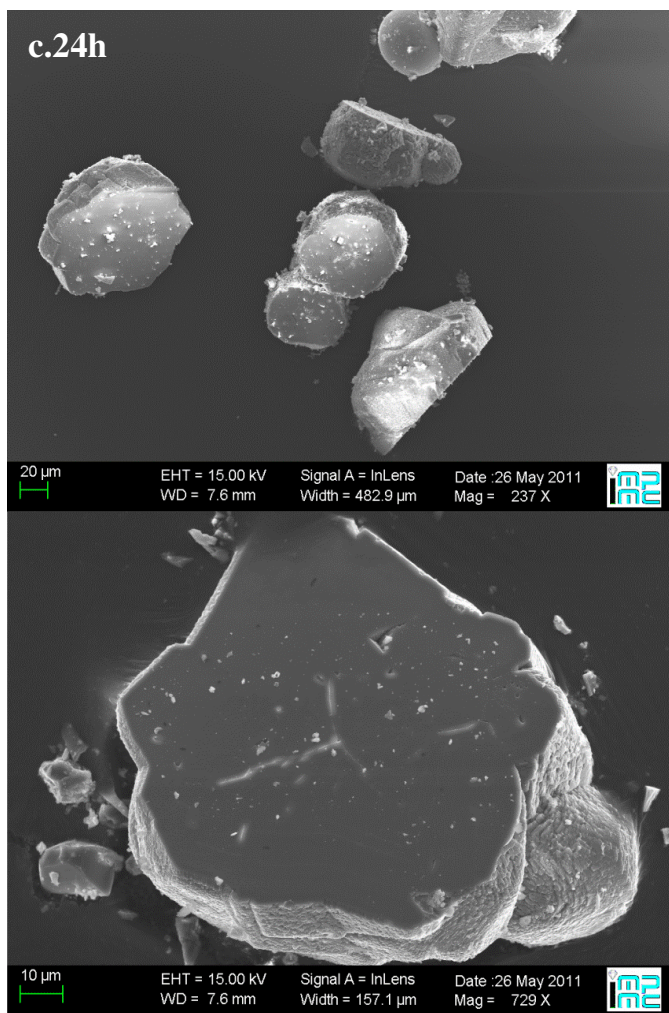


Fig. 3. (a, b, c, and d)

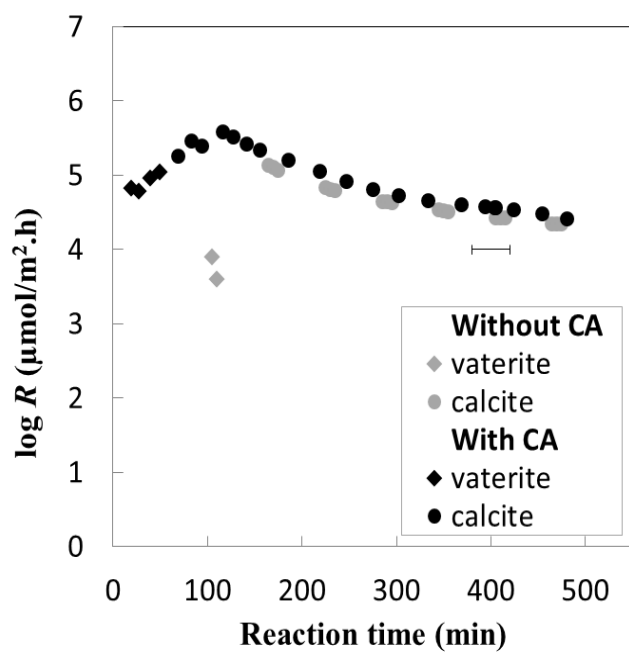


Fig. 4.

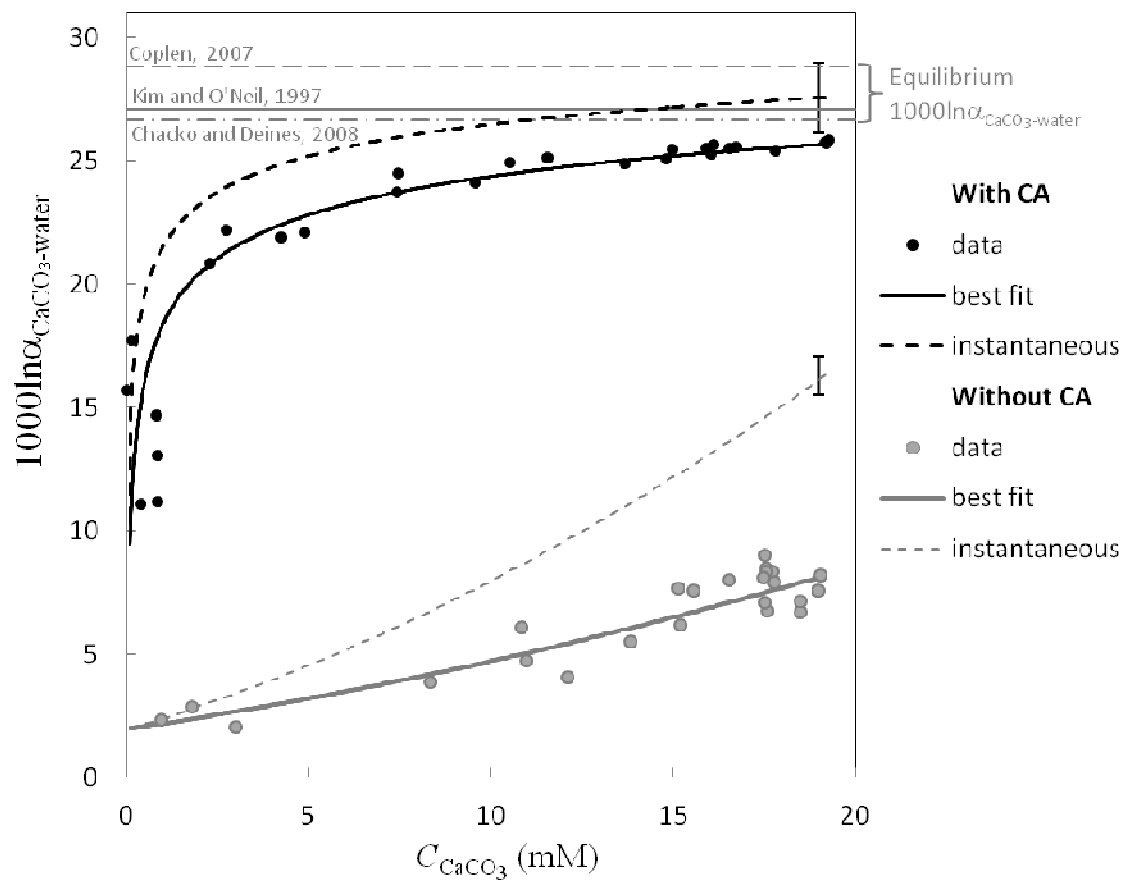


Fig. 5.

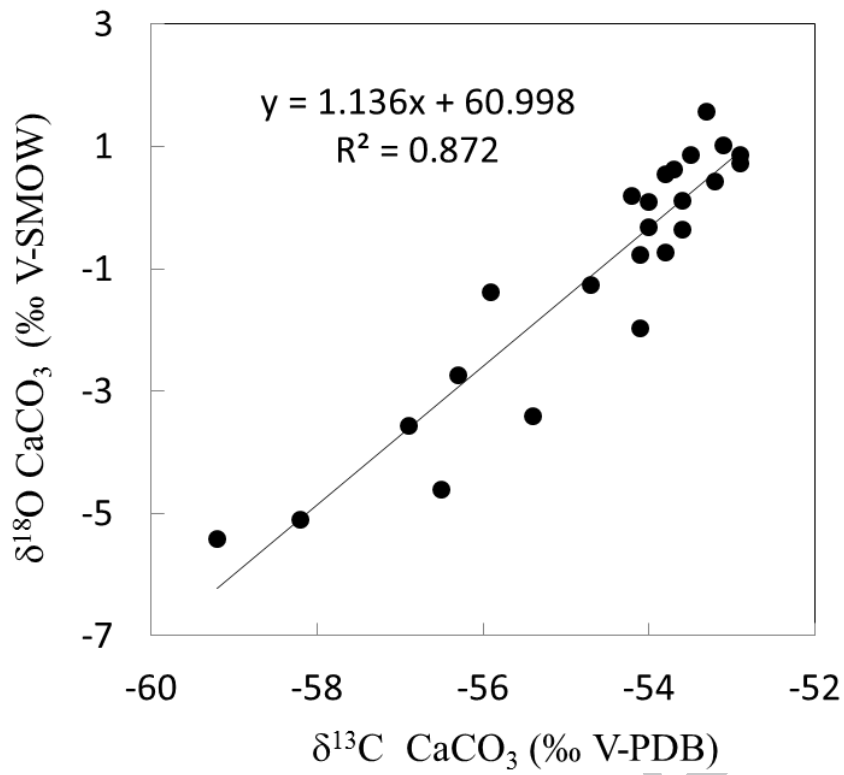


Fig.6.

## TABLES

Table 1. Chemical data and reaction parameters obtained for the experiment of CaCO<sub>3</sub> precipitation induced by *S. pasteurii* ureolysis in presence of carbonic anhydrase.

Reaction time (min)	[DIN] (mM) ( $\sigma = \pm 5\%$ )	Accumulated DIN (%) ( $\sigma = \pm 5\%$ )	$n_{\text{CaCO}_3}$ (mM) ( $\sigma = \pm 0.01$ )	% Precipitation ( $\sigma = \pm 0.05\%$ )	$\log R$ ( $\mu\text{mol}/\text{m}^2\text{h}$ )	$n_{\text{DIC}}$ (mM) ( $\sigma = \pm 5\%$ )	Blank-corrected $n_{\text{DIC}}^{\text{a}}$ (mM) ( $\sigma = \pm 5\%$ )	%AC (%) ( $\sigma = \pm 5\%$ )	pH ( $\sigma = \pm 0.01$ )
20	0.0	0.0	0.4	1.8	4.8	0.49	0.32	2.1	8.70
27	0.2	0.4	0.8	4.1	4.8	1.05	0.88	5.1	8.86
40	3.5	5.3	0.8	4.1	5.0	1.75	1.58	7.3	8.98
50	3.3	4.9	0.0	0.0	5.0	1.79	1.61	4.7	8.99
69	5.9	8.9	0.1	0.6	5.3	3.36	3.19	9.9	9.02
83	8.5	12.8	0.8	4.0	5.5	4.23	4.06	14.7	9.04
94	21.4	32.2	2.7	13.3	5.4	4.75	4.58	22.0	9.02
116	21.7	32.6	2.3	11.0	5.6	5.25	5.08	22.1	8.85
127	16.6	25.0	4.2	20.5	5.5	5.80	5.63	29.6	8.81
142	23.3	35.0	4.9	23.7	5.4	6.10	5.93	32.5	8.89
156	29.6	44.5	7.4	35.9	5.3	5.99	5.82	39.7	8.81
186	33.4	50.1	9.6	46.4	5.2	6.92	6.75	49.0	8.72
219	25.8	38.7	7.5	36.2	5.0	6.17	6.00	40.4	8.64
247	36.8	55.2	10.5	51.0	4.9	7.53	7.36	53.6	8.65
275	40.9	61.4	11.6	56.1	4.8	6.39	6.22	53.4	8.69
303	39.7	59.6	13.7	66.3	4.7	6.75	6.58	60.8	8.65
334	36.9	55.4	14.8	71.8	4.7	7.48	7.31	66.4	8.63
369	56.5	84.8	15.0	72.6	4.6	6.72	6.54	64.6	8.64
394	45.7	68.7	15.9	77.2	4.6	7.74	7.57	70.5	8.43
404	51.6	77.4	16.0	77.9	4.6	6.56	6.39	67.4	8.50
405	49.2	73.9	16.5	80.3	4.6	7.59	7.42	71.9	8.53
424	43.1	64.7	16.1	78.1	4.5	7.25	7.08	69.6	8.50
454	47.0	70.6	16.7	81.2	4.5	7.13	6.96	71.2	8.53
481	50.2	75.3	17.8	86.4	4.4	8.47	8.30	78.4	8.59
24 h	58.0	87.0	19.2	93.0	nd <sup>b</sup>	11.26	11.09	90.8	8.71
24 h	62.8	94.2	19.3	93.5	nd <sup>b</sup>	10.03	9.86	87.4	8.71
24 h	59.9	90.0	19.2	93.2	nd <sup>b</sup>	11.42	11.25	91.4	8.72

(a) Details on the blank correction procedure are given in Appendix B.3

(b) No data (precipitation had already ended)

Table 2. Oxygen isotope analysis of the two experiments of CaCO<sub>3</sub> precipitation induced by *S. pasteurii* ureolysis, with and without carbonic anhydrase.

Without carbonic anhydrase				With carbonic anhydrase			
Reaction time (min)	%AC (σ =	δ <sup>18</sup> O <sub>CaCO<sub>3</sub></sub> (‰ vs. V-SMOW)	δ <sup>18</sup> O <sub>H<sub>2</sub>O</sub> (‰ vs. V-SMOW)	Reaction time	%AC (σ =	δ <sup>18</sup> O <sub>CaCO<sub>3</sub></sub> (‰ vs. V-SMOW)	δ <sup>18</sup> O <sub>H<sub>2</sub>O</sub> (‰ vs. V-SMOW)
15	2	nd <sup>a</sup>	-7.5	20	2	4.3	nm <sup>b</sup>
20	2	nd <sup>a</sup>	-7.5	27	5	6.3	-7.0
25	3	nd <sup>a</sup>	-7.5	40	7	4.4	nm <sup>b</sup>
45	11	nd <sup>a</sup>	-7.4	50	5	9.0	nm <sup>b</sup>
50	12	nd <sup>a</sup>	-7.4	69	10	11.0	-6.8
55	10	nd <sup>a</sup>	-7.5	83	15	7.9	nm <sup>b</sup>
105	28	-5.1	-7.5	94	22	15.5	-6.8
110	38	-5.4	-7.4	116	22	14.2	nm <sup>b</sup>
115	26	-4.6	-7.6	127	30	15.3	nm <sup>b</sup>
165	76	-2.7	-7.4	142	32	15.4	nm <sup>b</sup>
170	78	-3.4	-7.1	156	40	17.1	nm <sup>b</sup>
175	59	-3.6	-7.6	186	49	17.5	nm <sup>b</sup>
225	82	-2.0	-7.4	219	40	17.9	nm <sup>b</sup>
230	76	-1.4	-7.5	247	54	18.3	-6.8
235	97	-1.3	-7.2	275	53	18.5	nm <sup>b</sup>
285	100	0.5	-7.3	303	61	18.3	-6.8
290	98	0.1	-7.4	334	66	18.4	nm <sup>b</sup>
295	92	0.2	-7.6	369	65	18.9	nm <sup>b</sup>
345	102	-0.7	-7.8	394	71	18.9	nm <sup>b</sup>
350	104	-0.4	-7.3	404	67	18.6	nm <sup>b</sup>
355	108	1.0	-7.3	405	72	18.9	-6.7
405	107	0.9	-7.3	424	70	19.0	nm <sup>b</sup>
410	103	1.6	-7.6	454	71	18.9	-6.6
415	109	0.4	-7.2	481	78	18.8	nm <sup>b</sup>
465	104	0.9	-7.2	24 h	91	19.1	-6.6
470	99	0.6	-7.6	24 h	87	19.2	-6.7
475	114	-0.8	-7.6	24 h	91	19.1	-6.8
24h	112	-0.3	-7.6				
24h	108	0.7	-7.5				
24h	110	0.1	-7.5				

(a) No data (precipitation had not yet become quantifiable).

(b) No measurements